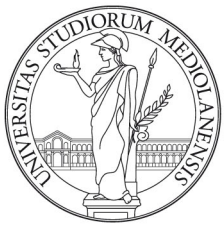

UNIVERSITÀ DEGLI STUDI DI MILANO
FACOLTÀ DI SCIENZE E TECNOLOGIE

DIPARTIMENTO DI FISICA

Cartan Metrology

Gabriele Fazio

994848

Relatore
Prof. Matteo G. A. Paris

Anno accademico 2023/2024

INTRODUCTION

This work is aimed at characterizing the kernel of a generic 2 qbit gate, obtained from the Cartan's decomposition. Specifically, our focus is on determining the limits to precision achievable in the joint estimation of the three parameters characterizing the Cartan's kernel. Subsequently, we want to also find the states that allow for such precision, and give a characterization of what makes a state sensible. Additionally, we seek to ascertain the robustness of optimal states against various kind of noises. Finally, we conclude finding simple suboptimal measures able to approximate optimal ones.

The first chapter provides a review of the postulates of quantum mechanics, with the relative extensions to open system. Some fundamental concepts of quantum computation, such as qbits and circuits, are also presented. The first chapter concludes with the formulation of Cartan's decomposition theorem and its application to elements of $SU(4)$.

The second chapter addresses the theory of multiparameter quantum metrology. Definitions of the symmetric logarithmic derivative, the quantum Fisher information matrix, and the Uhlmannn curvature are provided. Then the chapter concludes by stating the quantum Cramér-Rao bound.

The third chapter carries out the analysis, focusing on each of the previously stated objectives.

The main findings of this thesis may be summarized as follows. Two classes of states that provide respectively optimal and suboptimal performances has been found. The class of optimal states doesn't show a relation with respect to the concurrence. Then, it has been showed that these optimal states are robust against generic noise. And concluding, a measurement protocol has been provided, that allows precision close to optimal using local spin measurements on the two qbits.

TABLE OF CONTENTS

1

QUANTUM MECHANICS WITH TWO QBITS

1.1 QUANTUM MECHANICS

During the last century, a new theory to describe the behavior of objects at very small scales has emerged. We call this Quantum Mechanics. Quantum mechanics is a very broad theory, that can be used to describe a multitude of systems. Despite this, the fundamental formulation can be reduced to a few postulates, regarding respectively how to describe: states, measurements and the evolution.

1. The **state** of a quantum system is completely specified by a normalized state vector $|\psi\rangle$ living in a Hilbert space $\mathcal{H}$. Composite systems can be described by vectors living in the tensor product space $\mathcal{H}_1 \otimes \mathcal{H}_2 \otimes ...$ The **superposition principle** states that if $|\psi\rangle$ and $|\phi\rangle$ are possible states, then any normalized linear combination $\alpha|\psi\rangle + \beta|\phi\rangle$, with $\alpha, \beta \in \mathbb{C} \ : \ |\alpha|^2+|\beta|^2= 1$ is also a possible state.

2. There exists a linear hermitian operator for every observable. Such operator admits a spectral decomposition $O = \sum_k o_k |o_k\rangle\langle o_k|$, so that the states $|o_k\rangle$ form an orthonormal basis for the Hilbert space ($\langle o_j|o_k\rangle = \delta_{jk} \wedge \sum_k |o_k\rangle\langle o_k| = \mathbb{1}$). The result of a measurement is one of the $|o_k\rangle$ with probability given by the **Born rule** $P_k = |\langle o_k|\psi\rangle|^2$. After the measurement the state of the system becomes the $|o_k\rangle$ that has been observed.

3. The **evolution** of a state is given by a unitary operator, so that $|\psi(t)\rangle = U(t, t_0)|\psi(t_0)\rangle \ : \ U^\dagger U = \mathbb{1}$. If the Hamiltonian of the system is time independent we have $U(t, t_0) = e^{-iH(t-t_0)}$.

1.1.1 *Statistical Operator*

The description of states through vector elements of an Hilbert space, despite being effective, lacks generality. In fact if we don't have full control of the quantum system, noise or various kinds of phenomena could collapse the system casually. Thus, when we lack information about the system, a more effective description is given by the statistical (density) operator. If we represent the system as a statistical ensemble $\{p_k, |\psi_k\rangle\}$(with p_k the probability of being in the state $|\psi_k\rangle$, $\sum_k p_k = 1$, with in general $\langle\psi_l|\psi_m\rangle \neq 0$),we define the statistical operator as

$$\rho = \sum_k p_k \, |\psi_k\rangle \langle\psi_k| \, . \tag{1.1.1}$$

From this definition we can see it has various properties such as

- It is positive semi-definite, which follows from

$$\langle\phi|\rho|\phi\rangle = \sum_k p_k \langle\phi|\psi_k\rangle \langle\psi_k|\phi\rangle = \sum_k p_k |\langle\phi|\psi_k\rangle|^2 \geq 0 \tag{1.1.2}$$

  which is valid $\forall |\phi\rangle \in \mathcal{H}$.

- It has unit trace, which follows from

$$\mathrm{Tr}[\rho] = \sum_{j,k} p_k \langle e_j|\psi_k\rangle \langle\psi_k|e_j\rangle = \sum_k p_k \langle\psi_k|\psi_k\rangle = 1. \tag{1.1.3}$$

- It is Hermitian, which follows either from the definition, or from the fact that its eigenvalues must be real.

A statistical operator having only one nonzero eigenvalue is called **pure**, and it can be written as $\rho = |\psi\rangle\langle\psi|$. On the contrary, if a state has more eigenvalues, meaning it is a non trivial statistical ensemble, it is called **mixed**. Additionally, we can quantify the degree of purity with

$$\mu[\rho] = \mathrm{Tr}[\rho^2] \leq 1. \tag{1.1.4}$$

Where $\mu = 1$ represent a pure state, while a state is maximally mixed when $\mu = \frac{1}{n}$, with n the dimension of the Hilbert space. Therefore, in general we have $\frac{1}{n} \leq \mu \leq 1$.

1.1.2 *Quantum maps*

In an analogous way we can also extend the concept of evolution through quantum maps. For example a process that with different probabilities evolve with different hamiltonians, can't be described with just one unitary operator. An example of this is given by noisy channels. The unperturbed evolution is given by the identity matrix, but with a given probability p the evolution that describes the noise is applied. Formally a quantum map is a function

$$\mathcal{E}(\rho) = \rho'. \tag{1.1.5}$$

The requirements on the map are

1. It is **positive semi-definite** $\mathcal{E}(\rho) \geq 0$.
2. It is **trace non-increasing**, $0 \leq \mathrm{Tr}[\mathcal{E}(\rho)] \leq 1$, in order to also account for evolutions due to measurements.
3. It is a **completely positive** map, meaning that if we extend the action of the map in a wider space with $\mathcal{E} \otimes \mathbb{1}$, it is still positive semi-definite.

These constraints descend from the concept of unitarity. In order to see this, we can think of quantum maps as partial traces of unitary evolutions in larger Hilbert spaces. Calling A the system, and B the environment, we can see this fact from

$$\begin{aligned}\mathcal{E}(\rho_A) &= \mathrm{Tr}_B[U\rho_A \otimes \rho_B U^\dagger] = \sum_j p_j \mathrm{Tr}_B[U\rho_A \otimes |\rho_{B,j}\rangle\langle\rho_{B,j}| U^\dagger] \\ &= \sum_{j,k} p_j \langle e_k|U|\rho_{B,j}\rangle \rho_A \langle\rho_{B,j}|U^\dagger|e_k\rangle \equiv \sum_l M_l \rho_A M_l^\dagger,\end{aligned} \tag{1.1.6}$$

where it has been assumed the spectral decomposition $\rho_B = \sum_j p_j |\rho_{B,j}\rangle\langle\rho_{B,j}|$, and basis $\{|e_k\rangle\}$ for the B space. From this derivation we found what is referred to as the **Kraus decomposition**, that tells us that every quantum map is writable as $\mathcal{E}(\rho) = \sum_l M_l \rho M_l^\dagger$. From the above definition of $M_l \equiv \sqrt{p_j}\langle e_k|U|\rho_{B,j}\rangle$ (under a suitable reindexing $l = (j,k)$) it also follows the condition

$$\begin{aligned}\sum_l M_l^\dagger M_l &= \sum_{j,k} p_j \langle\rho_{B,j}|U|e_k\rangle\langle e_k|U|\rho_{B,j}\rangle \\ &= \sum_j p_j \langle\rho_{B,j}|U^\dagger U|\rho_{B,j}\rangle = \mathbb{1}.\end{aligned} \tag{1.1.7}$$

It has been proven that this formulation, and the 3 former requirements are equivalent.

Theorem 1 (Kraus-Choi-Sudarshan theorem)**.** *A quantum map $\mathcal{E}$ satisfies conditions 1-3, if and only if it is the partial trace of the evolution given by a unitary operator living in a larger Hilbert space(or equivalently if it possesses a Kraus decomposition $\mathcal{E}(\rho) = \sum_l M_l \rho M_l^\dagger$ so that $\sum_l M_l M_l^\dagger = \mathbb{1}$).*

1.2 QUANTUM BITS

Quantum bits, also called **qbits**, are the quantum extension of classical bits. A classical bit can be represented being in either a state 0 or a state 1. In a straightforward way we define qbits as systems that are described by a generic superposition of 0 and 1,

$$|\psi\rangle = \alpha\,|0\rangle + \beta\,|1\rangle\,. \tag{1.2.1}$$

With $\alpha, \beta \in \mathbb{C}$: $|\alpha|^2+|\beta^2|= 1$. A very useful isomorphism is the one which maps

$$|0\rangle \mapsto \begin{pmatrix} 1 \\ 0 \end{pmatrix},\ |1\rangle \mapsto \begin{pmatrix} 0 \\ 1 \end{pmatrix}, \tag{1.2.2}$$

with which a state can be written as a complex vector $|\psi\rangle \mapsto \begin{pmatrix} \alpha \\ \beta \end{pmatrix}$.

1.2.1 *Bloch sphere*

A useful representation of qbits can be given by the **Bloch sphere**. To get such representation we can firstly remove a global phase, making $\alpha \in [0, 1] \subset \mathbb{R}$. After this we can use the fact that the vector is normalized, to rewrite the module of the numbers with trigonometric functions as follows

$$|\psi\rangle = \cos(\frac{\theta}{2})\,|0\rangle + \sin(\frac{\theta}{2})e^{i\phi}\,|1\rangle\,, \tag{1.2.3}$$

with $\theta \in [0, \pi)$ and $\phi \in [0, 2\pi)$. This way we reduced the initial 4 free components of $\alpha, \beta \in \mathbb{C}$ to just 2 real numbers. Having two degree of freedom(thus a bidimensional domain), with the parameters being angles, we naturally think of an object like the

one in Figure 1.1. On the z-axis we have, on the north pole the state $|0\rangle$, and on the south pole the state $|1\rangle$.

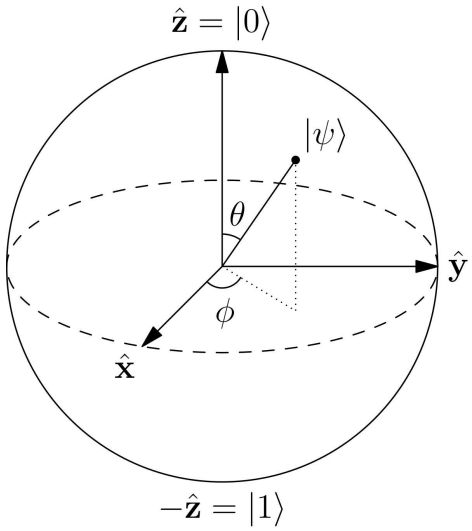

Fig. 1.1 Image of the Bloch sphere, the angles θ and ϕ corresponds to the parameters in the state parametrization given by the Equation 1.2.3.

An interesting property is that the length of the arrow doesn't need to be 1. In fact, given the Pauli matrices

$$\sigma_x \equiv \sigma_1 \equiv \begin{pmatrix} 0 & 1 \\ 1 & 0 \end{pmatrix}, \sigma_y \equiv \sigma_2 \equiv \begin{pmatrix} 0 & -i \\ i & 0 \end{pmatrix}, \sigma_z \equiv \sigma_3 \equiv \begin{pmatrix} 1 & 0 \\ 0 & -1 \end{pmatrix}, \tag{1.2.4}$$

in general we have that the 3D position of the arrow is given by

$$\underline{r} = \begin{pmatrix} \mathrm{Tr}[\sigma_x \rho] \\ \mathrm{Tr}[\sigma_y \rho] \\ \mathrm{Tr}[\sigma_z \rho] \end{pmatrix}. \tag{1.2.5}$$

It can be proved that the module of the vector is tied to the purity of an n dimensional space by

$$\mu[\rho] = \frac{1}{n}(1 + |\underline{r}|^2). \tag{1.2.6}$$

1.2.2 *Multiple qbits*

In general it is useful to work with more than one qbit. Given n qbits, the state of the whole system lives in the tensor product of the Hilbert spaces $\mathcal{H}^n = \bigotimes_{k=1}^{n} \mathcal{H}_k$. It is also useful some specific qbits notation, where the n bits can be represented as the string of bits, where usually the first qbit is positioned in the rightmost position. Given the set $b \equiv \{0, 1\}$ we can write

$$|b_{n-1}\rangle \otimes \ldots \otimes |b_0\rangle \equiv |b_{n-1}\ldots b_0\rangle \equiv |x_{10} = (b_{n-1}\ldots b_0)_2\rangle \in H^n \tag{1.2.7}$$

where sometimes, especially in summatories, it is useful to just refer to the base 10 value of the bit string.

In the specific case of two qbits in pure states, we can define a measure of entanglement between the two. We define the **concurrence** of state $|\psi\rangle = \sum_{x,y\in\{0,1\}} \alpha_{x,y} |x\rangle |y\rangle$ to be

$$C(|\psi\rangle) \equiv 2|\alpha_{00}\alpha_{11} - \alpha_{01}\alpha_{10}|. \tag{1.2.8}$$

This can be generalized for mixed states with $C(\rho) \equiv \max(0, \lambda_1 - \lambda_2 - \lambda_3 - \lambda_4)$, where $\lambda_1 \geq \lambda_2 \geq \lambda_3 \geq \lambda_4$ are the eigenvalues of operator $R \equiv \sqrt{\sqrt{\rho}(\sigma_y \otimes \sigma_y)\rho^*(\sigma_y \otimes \sigma_y)\sqrt{\rho}}$.

1.2.3 *Quantum Circuits*

When describing complex evolutions, or algorithms, that may involve classical controls in order to manipulate in specific ways a given system, it comes in useful a graphical representation.

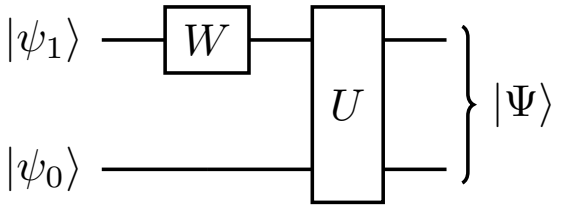

Fig. 1.2 Representation of a generic quantum circuit, where firstly a W gate is applied only to the second qbit, and then a U gate is applied on both qbits.

Quantum circuits are meant to be read from left to right. In general horizontal lines can correspond to different subsystems, but very often each line represent a different qbit. In particular the upper qbit is the leftmost in the bit string, and the lowest is the rightmost. On the left, initial states are represented, and on the right there are the final ones. Evolutions, also referable as gates, are represented by rectangles that act on some lines, which tells which qbits are involved in the evolution(the other qbits will undergo no evolution). For example Figure 1.2 is the representation of the evolution given by

$$|\psi_1\rangle |\psi_0\rangle \mapsto U(W \otimes \mathbb{1}) |\psi_1\rangle |\psi_0\rangle = |\Psi\rangle \tag{1.2.9}$$

To be noted how in general it is not possible to write for each qbit its own state, like it has been done at the start of Figure 1.2. In general a state of n qbits can be entangled, and if so it is not possible to factorize the state as a tensor product of various single qbit states. If a state is not entangled it is said to be **factorizable**.

1.3 CARTAN'S DECOMPOSITION

Let's now approach a core topic of the thesis, the Cartan decomposition. Let's consider a generic unitary gate acting on 2 qbits. Such evolution is given by a linear operator in $SU(4)$. Élie Joseph Cartan proved the following theorem

Theorem 2 (Cartan's KAK decomposition)**.** *Given a group $\underline{G} = exp(\underline{g})$, with a subgroup $\underline{K} = exp(\underline{k})$, and a Cartan subalgebra $\underline{a}$, where $\underline{g} = \underline{k} \oplus \underline{k}^{\perp}$ and $\underline{a} \subset \underline{k}^{\perp}$.*
Then any $G \in \underline{G}$ can be written as $G = K_1 A K_2$, with $K_1, K_2 \in \underline{K}$ and $A \in exp(\underline{a})$.

A special case of this theorem has been developed by Khaneja and Glaser for quantum computing. For additional details [1] provides a constructive proof using only linear algebra, of what is referred as KAK1 theorem.

Theorem 3 (Khaneja and Glaser's KAK1 theorem)**.** *Given any $S \in SU(4)$, there exists $A_0, A_1, B_0, B_1 \in SU(2)$, and $\underline{k} \in \mathbb{R}^3$, such that*

$$S = (A_1 \otimes A_0) e^{i\underline{k}\cdot\underline{\Sigma}} (B_1 \otimes B_0) \tag{1.3.1}$$

where $\Sigma \equiv \begin{pmatrix} \sigma_x \otimes \sigma_x \\ \sigma_y \otimes \sigma_y \\ \sigma_z \otimes \sigma_z \end{pmatrix} \equiv \begin{pmatrix} \sigma_{XX} \\ \sigma_{YY} \\ \sigma_{ZZ} \end{pmatrix}$.

Starting from a generic operator over $\mathbb{C}^4$, which has 16 free components, unitarity reduces the degrees of freedom only by 1. One of the strengths of this theorem is the ability to separate the contribute of all these different parameters. In fact what we see is that only 3 of the initial 15 parameters are involved in the interaction between the two qbits. The other 12 are then only single qbit evolutions. This decomposition is depicted in Figure 1.3.

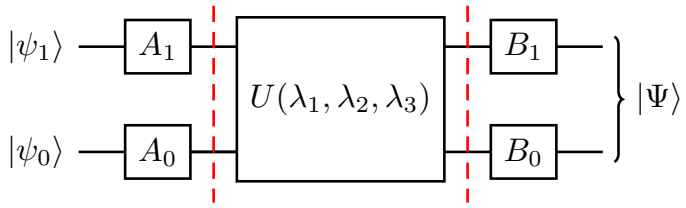

Fig. 1.3 The decomposition of a generic gate can be made through couples of single qbit operations with an interaction gate in the middle.

The U gate is also called the **Cartan's kernel**, and will be the main object of our analysis.

1.3.1 *Cartan's kernel*

The Theorem 3 provides us an analytical expression for the gate U.

$$U = e^{i\underline{k}\cdot\underline{\Sigma}} = e^{i\sum_j k_j(\sigma_j\otimes\sigma_j)} = e^{i\sum_j k_j\sigma_{jj}} \tag{1.3.2}$$

For the sake of correspondence with an hamiltonian, we may want to make the exponent in the form $-iH$, therefore we can rename the variable $\underline{k}$ with $\underline{\lambda} \equiv -\underline{k}$.

We now derive its matrix representation. A possible approach to proceed analytically is diagonalizing the exponent, exponentiating, and then going back to the original base. Doing this we get

$$U = e^{-i\sum_j \lambda_j\sigma_{jj}} = \begin{pmatrix} e^{-i\lambda_3}\cos(\lambda_1-\lambda_2) & 0 & 0 & -ie^{-i\lambda_3}\sin(\lambda_1-\lambda_2) \\ 0 & e^{i\lambda_3}\cos(\lambda_1+\lambda_2) & -ie^{i\lambda_3}\sin(\lambda_1+\lambda_2) & 0 \\ 0 & -ie^{i\lambda_3}\sin(\lambda_1+\lambda_2) & e^{i\lambda_3}\cos(\lambda_1+\lambda_2) & 0 \\ -ie^{-i\lambda_3}\sin(\lambda_1-\lambda_2) & 0 & 0 & e^{-i\lambda_3}\cos(\lambda_1-\lambda_2) \end{pmatrix}. \tag{1.3.3}$$

A subtle but crucial thing to note is that the basis that diagonalize is the Bell basis. Where, given the states in the Bell basis with $j, k \in \{0, 1\}$, their corresponding expression in the canonical base is

$$\left(|\beta_{jk}\rangle \right)_B = \left(\frac{|0\rangle |k\rangle + (-1)^j |1\rangle |\bar{y}\rangle}{\sqrt{2}} \right)_C . \tag{1.3.4}$$

In the Bell basis the kernel assumes the form

$$U = \begin{pmatrix} e^{-i(\lambda_1 - \lambda_2 + \lambda_3)} & 0 & 0 & 0 \\ 0 & e^{-i(\lambda_1 + \lambda_2 - \lambda_3)} & 0 & 0 \\ 0 & 0 & e^{i(\lambda_1 - \lambda_2 - \lambda_3)} & 0 \\ 0 & 0 & 0 & e^{i(\lambda_1 + \lambda_2 + \lambda_3)} \end{pmatrix}_B . \tag{1.3.5}$$

The last thing to be discussed about the decomposition is the domain of the parameters. We initially have that $\lambda_j \in [0, 2\pi) \in \mathbb{R}$. Then, we can define an equivalence relation, where two kernels $U, V \in SU(4)$ are said to be **equivalent up to local operations**, if there exists $R_0, R_1, L_0, L_1 \in U(2)$ such that $U = (R_1 \otimes R_0)V(L_1 \otimes L_0)$. It can be proven that this is a valid equivalence relation. Starting from this we can find three operations on k that preserve the equivalence class.

1. **Shift**: $\underline{\lambda}$ can be shifted on any of the three components by an integer multiple of $\frac{\pi}{2}$. So given $n, m, l \in \mathbb{Z}$.

$$(\lambda_x, \lambda_y, \lambda_z) \mapsto (\lambda_x + n\frac{\pi}{2}, \lambda_y + m\frac{\pi}{2}, \lambda_z + l\frac{\pi}{2}) \tag{1.3.6}$$

2. **Reverse**: any two components can change sign. For example

$$(\lambda_x, \lambda_y, \lambda_z) \mapsto (-\lambda_x, -\lambda_y, \lambda_z) \tag{1.3.7}$$

3. **Swap**: any two components can be swapped. For example

$$(\lambda_x, \lambda_y, \lambda_z) \mapsto (\lambda_y, \lambda_x, \lambda_z) \tag{1.3.8}$$

Using these operation it is possible to reduce the domain to what is called the **canonical class vector set**.

$$D = \{\underline{\lambda} \in \mathbb{R}^3 \ : \ \frac{\pi}{2} > \lambda_x \geq \lambda_y \geq \lambda_z \geq 0 \wedge \lambda_x + \lambda_y \leq \frac{\pi}{2}\} \tag{1.3.9}$$

The algorithm to reduce $\mathbb{R}^3$ into D is described in [1]. This said, for simplicity in some numeric calculations the domain has been considered to be $[0, 2\pi)$.

2

MULTIPARAMETER QUANTUM METROLOGY

There exists interesting quantities of given quantum systems that aren't directly observable. Either because they aren't associated with proper quantum observables, or because of experimental impediments. Two remarkable examples are the entanglement and purity, both nonlinear functions of the statistical operator, and thus not possessing corresponding observables. Therefore, to measure such quantities we resort to indirect statistical methods, inferring information from sets of data, corresponding to observables different from the one of interest.

The cases of single parameter, and multiparameter estimation, despite having common features, differ for fundamental reasons. A first important reason is that in quantum mechanics there may be measures which are non compatible. When this is the case, optimal estimability of all parameters is impossible without some kind of trade-off. Additionally there may be correlations between the parameters. All this can be in general handled with weight matrices that optimizes precision under given cost functions.

2.1 RELEVANT QUANTITIES

Let's start formalizing the approach through the derivation of some important objects.

2.1.1 *Symmetric Logarithmic Derivative*

The **symmetric logarithmic derivative**(SLD) is implicitly defined by

$$\partial_{\lambda_j}\rho \equiv \partial_j\rho \equiv \frac{L_{\lambda_j}\rho + \rho L_{\lambda_j}}{2} \equiv \frac{L_j\rho + \rho L_j}{2}, \tag{2.1.1}$$

where the subscript j corresponds to the derivative with respect to the j-th parameter λ_j. In the case of pure states the solution is trivial. By observing that $\rho^2 = \rho$ we get

$$\partial_j\rho = \partial_j(\rho^2) = (\partial_j\rho)\rho + \rho(\partial_j\rho). \tag{2.1.2}$$

Comparing Equations 2.1.1 and 2.1.2 we see that a solution is given by

$$L_j = 2\partial_j\rho. \tag{2.1.3}$$

2.1.2 *Classical and Quantum Fisher information matrix*

Classically we have that given a set of parameters to be estimated $\underline{\lambda}$, and a measure x, we have a conditional probability $p(x|\underline{\lambda})$. From this the Fisher information matrix is defined to be

$$F_{jk} = \sum_x \frac{\partial_j p(x|\underline{\lambda})\ \partial_k p(x|\underline{\lambda})}{p(x|\underline{\lambda})}, \tag{2.1.4}$$

where if we have a quantistic system $p(x|\underline{\lambda}) = |\langle x|\psi_{\underline{\lambda}}\rangle|^2$.

From the classical Fisher information matrix it is possible to derive a quantistic counterpart. The **quantum fisher information matrix**(QFI) $[Q]_{jk}$ is defined via the SLD by

$$Q_{jk} \equiv \mathrm{Tr}\left[\rho\frac{L_jL_k + L_kL_j}{2}\right] = \frac{1}{2}\mathrm{Tr}[\rho\{L_j, L_k\}] \tag{2.1.5}$$

Since in general it may be difficult to solve for L, we can express the QFI in terms of the eigenvalues and eigenvectors of the statistical operator. This formulation is provided by Theorem 2.2 in [2], which will be reported here.

Theorem 4. *Given the spectral decomposition of a density matrix* $\rho = \sum_{\lambda_j\in S}\lambda_j|\lambda_j\rangle\langle\lambda_j|$, *where* $S = \{\lambda_j \in \{\lambda_j\} \ :\ \lambda_j \neq 0\}$ *is the support of non null eigenvalues. Then* Q_{jk} *is given*

by

$$\begin{aligned} Q_{jk} = \sum_{\lambda_l \in S} \left(\frac{(\partial_j \lambda_l)(\partial_k \lambda_l)}{\lambda_l} + 4\lambda_l \mathrm{Re}[\langle \partial_j \lambda_l | \partial_k \lambda_l \rangle] \right) \\ - \sum_{\lambda_l, \lambda_m \in S} \frac{8\lambda_l \lambda_m}{\lambda_l + \lambda_m} \mathrm{Re}[\langle \partial_j \lambda_l | \lambda_m \rangle \langle \lambda_m | \partial_k \lambda_l \rangle]. \end{aligned} \tag{2.1.6}$$

A last useful reformulation of the QFI is the one in the limit of pure states(i.e. $\rho_{\underline{\lambda}} = |\psi\rangle\langle\psi|$). By putting Equation 2.1.3 into the definition 2.1.5 we get

$$Q_{jk} = 4[\langle \partial_j \psi | \partial_k \psi \rangle - \langle \partial_j \psi | \psi \rangle \langle \psi | \partial_k \psi \rangle]. \tag{2.1.7}$$

The QFI is an important object because it gives us some relevant quantities. Firstly we have that its determinant is related to the amount of information we have on the parameters we're trying to estimate. For example, if the determinant is null, we could have that the parameters are not independent, and thus it can tell us if we are overparametrizing the problem. A second important quantity is the trace of the inverse. In the next section(2.2) it will be more clear why, but this quantity is related to the lower bound of the sum of the variances of the three parameters.

2.1.3 *Uhlmann curvature*

Similarly to the QFI the **Uhlmann curvature**, also called **incompatibility matrix** is defined via the SLD, but instead of using the anticommutator as in Equation 2.1.5, the commutator is used.

$$D_{jk} \equiv -i\mathrm{Tr}\left[\rho \frac{L_j L_k - L_k L_j}{2}\right] = -\frac{i}{2}\mathrm{Tr}[\rho[L_j, L_k]] \tag{2.1.8}$$

From the definition we see that the main diagonal is always made of zeros. The meaning of the off diagonal terms is related to the quantum incompatibility. Therefore, if we have $D = 0$, what we deduce is that all parameters are compatible. As stated in [3], if $D = 0$ the model is said to be **asymptotically classical**. In this case the optimal estimation is asymptotically achievable via collective measurements on $\rho_{\underline{\lambda}}^{\otimes n} \equiv \bigotimes_{j=1}^{n} \rho_{\underline{\lambda}}$ with $n \to +\infty$, $\rho_{\underline{\lambda}} \equiv U\rho_0 U^\dagger$, and ρ_0 the initial state.

2.2 QUANTUM CRAMÉR-RAO BOUND

Let's now approach a core inequality of quantum multiparameter estimation theory, the **quantum Cramér-Rao bound**(CRB), which is the quantum analogue of the classical Cramér-Rao bound. Let's define $\hat{\underline{\lambda}} \equiv \hat{\underline{\lambda}}(\{x_j\})$ as an estimator that maps a given set of measurements into the space of parameters. We assume this to be unbiased, meaning $\langle \hat{\underline{\lambda}} \rangle = \langle \underline{\lambda} \rangle$. Given the covariance matrix $\mathrm{Cov}[\hat{\underline{\lambda}}]_{jk} \equiv \langle \hat{\lambda}_j \hat{\lambda}_k \rangle - \langle \hat{\lambda}_j \rangle \langle \hat{\lambda}_k \rangle$, and the number of measurements M, the multiparameter Cramér-Rao bound states that

$$\mathrm{Cov}[\underline{\lambda}] \geq \frac{Q^{-1}}{M}, \tag{2.2.1}$$

with Q the quantum fisher information matrix.

If we want to estimate the precision with which we can determine the parameters, we can use as a relevant statistical quantity the trace of the covariance matrix. By doing so we see that

$$\mathrm{Tr}[\mathrm{Cov}[\underline{\lambda}]] \geq \frac{\mathrm{Tr}[Q^{-1}]}{M}. \tag{2.2.2}$$

This tells us that $\mathrm{Tr}[Q^{-1}]/M$, or in the asymptotic case of many measures $\mathrm{Tr}[Q^{-1}]$, gives us the lower bound we can get for $\mathrm{Tr}[\mathrm{Cov}[\underline{\lambda}]]$. Thus explaining the precedent claim of $\mathrm{Tr}[Q^{-1}]$ being the optimal precision achievable(asymptotically).

3

CARTAN METROLOGY

Let's now state the main objective of the thesis. Given a certain 2 qbit gate, we want to be able to estimate the parameters that describe it. In particular, as mentioned in Theorem 3, we can always decompose a 2 qbits gate into single qbit operations, and a kernel acting on 2 qbits. The focus of the thesis will be on this latter gate, being the one characterizing the interaction between 2 qbits. As already mentioned the Cartan's kernel is dependent on 3 parameters $\underline{\lambda}$, which we will be looking for.

The objectives are

1. Looking for optimal and suboptimal precision achievable.
2. Looking for states that allow such precision.
3. Looking for robustness of such states under noise.
4. Looking for the measures that allow such optimal, and a suboptimal precision.

The following analysis will be performed on qbits, assuming that initial states are prepared as pure states. For an alternative, but brief analysis on qtrits(a pair of three level systems), refer to Appendix B.

Before diving into the analysis, let's discuss a first hypothesis which set the initial direction of the analysis, despite later on turning out to be false.

Since the kernel is the entangling part of a given 2 qbit gate, we may be led into making two observations. The first is that factorizable states may be more sensible to the entanglement, and thus be able to yield better precision. A second observation, tied to the prior, is that more entangling gates could lead to more precise estimates of $\underline{\lambda}$. This, because if we put factorized states in a gate that has a high entangling power, we may expect that to be the most ideal case, since we may be dealing with a

highly sensible system. Later on we will see where and why this first view is wrong.

As a side note, for the mentioned reasons, it has also been done a quick analysis on the entangling power of the U gate, at various $\underline{\lambda}$. For further details refer to Appendix A.

3.1 OPTIMIZATION IN THE CANONICAL BASE PARAMETRIZATION

3.1.1 *Quantum Fisher information matrix*

Let's begin the analysis by calculating the QFI matrix. First of all we need $|\psi_{\underline{\lambda}}\rangle \equiv U|\psi_0\rangle$. To calculate this we need to parametrize a generic state. This can be easily done using the canonical base by

$$|\psi_0\rangle \equiv \begin{pmatrix} \alpha \\ \beta e^{i\phi_\beta} \\ \gamma e^{i\phi_\gamma} \\ \delta e^{i\phi_\delta} \end{pmatrix}, \tag{3.1.1}$$

with $\alpha, \beta, \gamma, \delta \in [0, 1]$, and $\phi_\beta, \phi_\gamma, \phi_\delta \in [0, 2\pi)$ such that $\alpha^2 + \beta^2 + \gamma^2 + \delta^2 = 1$. To be noted how from now on greek letters will correspond to the parametrization in the canonical base.

After this we take the U defined in Equation 1.3.3, and by applying it on $|\psi_0\rangle$ we get

$$|\psi_{\underline{\lambda}}\rangle = \begin{pmatrix} e^{-i\lambda_3}\left[\alpha\cos(\lambda_1-\lambda_2) - i\delta e^{i\phi_\delta}\sin(\lambda_1-\lambda_2)\right] \\ e^{i\lambda_3}\left[\beta e^{i\phi_\beta}\cos(\lambda_1+\lambda_2) - i\gamma e^{i\phi_\gamma}\sin(\lambda_1+\lambda_2)\right] \\ e^{i\lambda_3}\left[\gamma e^{i\phi_\gamma}\cos(\lambda_1+\lambda_2) - i\beta e^{i\phi_\beta}\sin(\lambda_1+\lambda_2)\right] \\ e^{-i\lambda_3}\left[\delta e^{i\phi_\delta}\cos(\lambda_1-\lambda_2) - i\alpha\sin(\lambda_1-\lambda_2)\right] \end{pmatrix}. \tag{3.1.2}$$

We now want to calculate the QFI. Since we're dealing with pure states we can take the simpler form provided by Equation 2.1.7, from which we get

$$Q = \begin{pmatrix} Q_{11} & Q_{12} & Q_{13} \\ Q_{21} & Q_{22} & Q_{23} \\ Q_{31} & Q_{32} & Q_{33} \end{pmatrix} \tag{3.1.3}$$

with

$$
\begin{aligned}
Q_{11} &= 4\Big[\alpha^2\left[1-2\delta^2\right]-2\alpha\delta\left[\alpha\delta\cos\left(2\phi_\delta\right)+4\beta\gamma\cos\left(\phi_\delta\right)\cos\left(\phi_\beta-\phi_\gamma\right)\right] \\
&\quad -2\beta^2\gamma^2\cos\left(2(\phi_\beta-\phi_\gamma)\right)-2\beta^2\gamma^2+\beta^2+\gamma^2+\delta^2\Big] \\
Q_{22} &= 4\Big[\alpha^2\left[1-2\delta^2\right]-2\alpha\delta\left[\alpha\delta\cos\left(2\phi_\delta\right)-4\beta\gamma\cos\left(\phi_\delta\right)\cos\left(\phi_\beta-\phi_\gamma\right)\right] \\
&\quad -2\beta^2\gamma^2\cos\left(2(\phi_\beta-\phi_\gamma)\right)-2\beta^2\gamma^2+\beta^2+\gamma^2+\delta^2\Big] \\
Q_{33} &= 4\Big[-\left[(\alpha-1)\alpha-\beta^2-\gamma^2+\delta^2\right]\left[\alpha^2+\alpha-\beta^2-\gamma^2+\delta^2\right]+\beta^2+\gamma^2+\delta^2\Big] \\
Q_{12} &= Q_{21} = 4\Big[2\alpha^2\delta^2\cos\left(2\phi_\delta\right)+\left(2\alpha^2-1\right)\delta^2-\alpha^2-2\beta^2\gamma^2\cos\left(2(\phi_\beta-\phi_\gamma)\right) \\
&\quad -2\beta^2\gamma^2+\beta^2+\gamma^2\Big] \\
Q_{13} &= Q_{31} = 8\Big[\beta\gamma\left[-\alpha^2+\beta^2+\gamma^2-\delta^2-1\right]\cos\left(\phi_\beta-\phi_\gamma\right) \\
&\quad +\alpha\delta\cos\left(\phi_\delta\right)\left[-\alpha^2+\beta^2+\gamma^2-\delta^2+1\right]\Big] \\
Q_{23} &= Q_{32} = 8\Big[\beta\gamma\left[-\alpha^2+\beta^2+\gamma^2-\delta^2-1\right]\cos\left(\phi_\beta-\phi_\gamma\right) \\
&\quad +\alpha\delta\cos\left(\phi_\delta\right)\left[\alpha^2-\beta^2-\gamma^2+\delta^2-1\right]\Big]
\end{aligned}
\tag{3.1.4}
$$

Despite being seemingly complex, we get symmetrical and relatively simple expressions for its determinant, and the trace of its inverse

$$
\mathrm{Tr}[Q^{-1}] = \frac{3}{16}\left(\frac{\alpha^2+\delta^2}{\alpha^4-2\alpha^2\delta^2\cos\left(2\phi_\delta\right)+\delta^4}+\frac{\beta^2+\gamma^2}{\beta^4-2\beta^2\gamma^2\cos\left(2(\phi_\beta-\phi_\gamma)\right)+\gamma^4}\right), \tag{3.1.5}
$$

$$
\mathrm{Det}[Q] = 1024\left[\alpha^4+\delta^4-2\alpha^2\delta^2\cos\left(2\phi_\delta\right)\right]\left[\beta^4+\gamma^4-2\beta^2\gamma^2\cos\left(2(\phi_\beta-\phi_\gamma)\right)\right]. \tag{3.1.6}
$$

A very remarkable observation that can be made here is that both trace and determinant are not functions of $\underline{\lambda}$. There are a few implications for this fact. A first one is that every $\underline{\lambda}$ can be estimated with equal precision. The second is that, since every $\underline{\lambda}$ allows for equal precision, even when $\underline{\lambda} = \underline{0}$(meaning $U = \mathbb{1}$), we can achieve optimality(more generally optimality is achievable independently of the entangling power). This gives us an initial indication that our first hypothesis is wrong. In fact if precision is independent of the ability to entangle of U, then the factorizability is probability not a feature necessary for optimal states. In fact in the case $U = \mathbb{1}$ we have no entanglement, and yet we achieve optimal precision.

3.1.2 *Uhlmann curvature*

Before diving into the optimization let's have a brief excursus regarding the Uhlmann curvature. Using Equation 2.1.8 we can calculate D, and by doing so we find that $D = 0$. As mentioned in Section 2.1.3, this imply that our model is asymptotically classical, meaning that the CRB is asymptotically saturable. Additionally this also tells us that all parameters are compatible, and thus there is no additional noise due to quantum incompatibility.

3.1.3 *State optimization*

A first thing we may want to do is get an idea of how trace and determinant are related. By sampling numerically random states, we can plot the trace and determinant of their QFI, given from Equations 3.1.5 and 3.1.6. The result is presented in Figure 3.1, where points on the determinant-trace plane has been plotted, sampling from a uniform distribution.

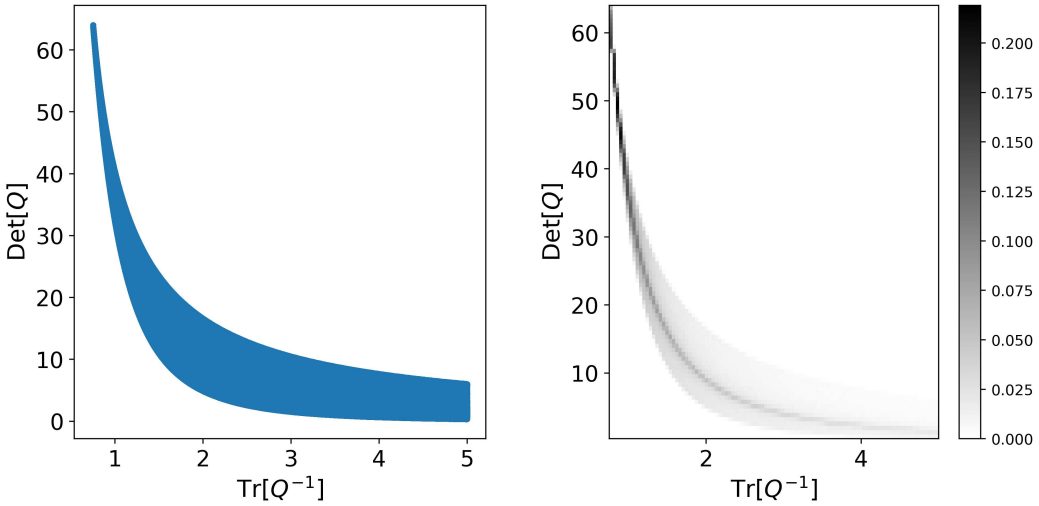

Fig. 3.1 Image on the trace-determinant plane formed by uniformly sampling (2 million)states and applying Equations 3.1.5 and 3.1.6. The left panel shows the image set, while the right one shows the density of states at given Tr-Det. For graphical reasons the trace has been limited for values below 5, in reality the trace is unbounded.

A first thing we see is that the determinant ranges from 64, to 0(asymptotically). The trace goes instead from minTr = $\frac{3}{4}$, up to infinity. In the graph we can see a relation where, a higher determinant(more information) is related to a smaller

trace(better precision). Furthermore, we see that the optimal point at $\left(\frac{3}{4}; 64\right)$ both maximizes determinant and minimize the trace at the same time.

To find the states that give the optimal point, and to also verify the numerical value found, we can either optimize the trace or the determinant, since optimal states optimize both. For simplicity we report Equation 3.1.6, which can be rewritten as

$$\begin{aligned} \mathrm{Det}[Q] = 1024\Big[\left[\alpha^2+\delta^2\right]^2 - 2\alpha^2\delta^2\left[1+\cos\left(2\phi_\delta\right)\right]\Big]\times \\ \Big[\left[\beta^2+\gamma^2\right]^2 - 2\beta^2\gamma^2\left[1+\cos\left(2(\phi_\beta-\phi_\gamma)\right)\right]\Big]. \end{aligned} \tag{3.1.7}$$

The expression is made up of two terms, each dependent on a different phase. In order to maximize the product we can maximize the singular terms with an opportune phase. We can see that the third term is always negative, thus the maximum it can assume is 0, when $\cos(x) = -1$. Alternatively, it may also be that either α or δ, and either β or γ are 0. These two options will characterize two classes of solutions.

Having cancelled the third term, the terms $(\alpha^2+\delta^2)$ and $(\beta^2+\gamma^2)$ remains. Given this, a good change of variable that accounts for normalization is given by imposing $\alpha^2+\delta^2 = \sin^2(\theta)$ and $\beta^2+\gamma^2 = \cos^2(\theta)$. By doing so we get

$$\mathrm{Det}[Q] = 1024\sin^4(\theta)\cos^4(\theta) = 64\sin^4(2\theta), \tag{3.1.8}$$

where opportune trigonometric identities have been used. This way it is evident that we have optimal states for $\sin(2\theta) = 1$. Additionally we confirmed that $\max \mathrm{Det}[Q] = 64$. From this derivation we get the following optimal states

$$|\psi_{\text{factorizable}}\rangle \in \left\{ \begin{pmatrix} \frac{1}{\sqrt{2}} \\ \frac{1}{\sqrt{2}}e^{i\phi} \\ 0 \\ 0 \end{pmatrix}, \begin{pmatrix} \frac{1}{\sqrt{2}} \\ 0 \\ \frac{1}{\sqrt{2}}e^{i\phi} \\ 0 \end{pmatrix}, \begin{pmatrix} 0 \\ \frac{1}{\sqrt{2}}e^{i\phi} \\ 0 \\ \frac{1}{\sqrt{2}} \end{pmatrix}, \begin{pmatrix} 0 \\ 0 \\ \frac{1}{\sqrt{2}}e^{i\phi} \\ \frac{1}{\sqrt{2}} \end{pmatrix} \right\} \tag{3.1.9}$$

$$|\psi_{\text{entangled}}\rangle = \begin{pmatrix} \alpha \\ \beta e^{i\phi} \\ \pm i\sqrt{\frac{1}{2} - \beta^2} e^{i\phi} \\ \pm i\sqrt{\frac{1}{2} - \alpha^2} \end{pmatrix} \tag{3.1.10}$$

with $\alpha, \beta \in [0, \frac{1}{\sqrt{2}}]$.

The first class of solutions are factorizable states, which are basically reducible to opportune combinations of a qbit being in a superposition of 0 and 1 with equal probability, and the other in either $|1\rangle$ or $|0\rangle$.

The second class of solutions spans all possible concurrences from 0 to 1. We can see that not only they have non null intersection, but the first class is contained in the second. Nevertheless it is interesting keeping them separate since they have different characteristics.

Concluding the optimization, formally, one may also need to prove that minimum trace corresponds to maximum determinant. This since the real optimization has to be on the trace and not the determinant. But it can be easily seen that the optimization of the trace is quite similar to the one on the determinant. In fact under the same assumptions of choosing an opportune phase, and same reparametrization in θ we get from Equation 3.1.5

$$\text{Tr}[Q^{-1}] = \frac{3}{16}\left(\frac{1}{\sin^2(\theta)} + \frac{1}{\cos^2(\theta)}\right) = \frac{3}{16}\frac{1}{\sin^2(\theta)\cos^2(\theta)} = \frac{3}{4\sin^2(2\theta)}. \tag{3.1.11}$$

This gives the same solutions, already presented in Equations 3.1.9 and 3.1.10.

3.1.4 *Entanglement is not a resource*

Having found optimal solutions, we can now better address the hypothesis that factorizable states could act as more sensible probes. By plotting the points from all states in blue, and the factorizable states in orange, we can compare how they behave in relation to the others. This is shown in Figure 3.2.

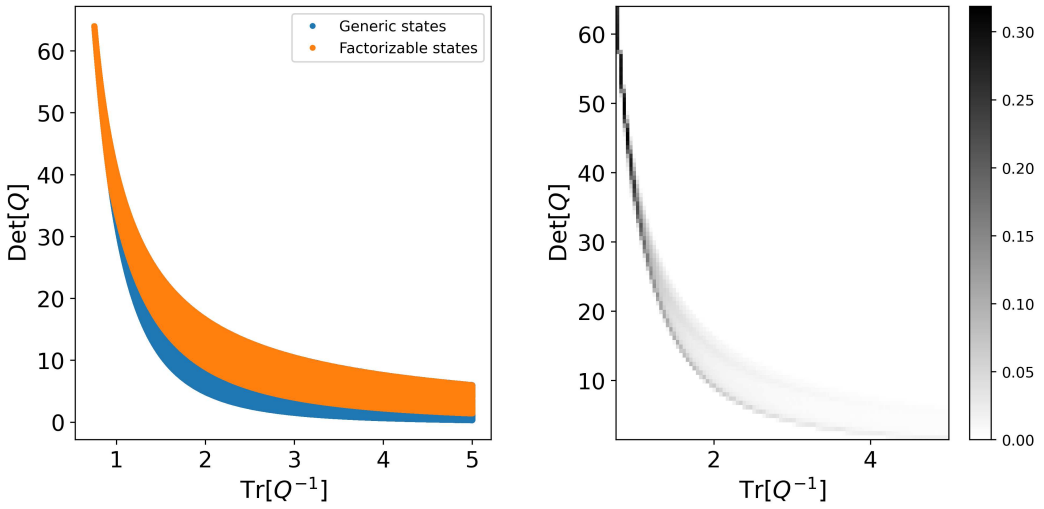

Fig. 3.2 Left panel shows the trace-determinant plane formed by uniformly sampling (2 million)states in blue, and (2 million)factorizable states in orange. The right panel shows the density of factorizable states at given Tr-Det. For graphical reasons the trace has been limited for values below 5, in reality the trace is unbounded. Despite not being visible, the blue band is always below the orange. This since they are all possible states, and thus containing all the factorized ones too.

What we see is that, despite not having anymore the lower part, we still get pretty much the same image, and once again we have a higher density of states along the same middle curve.

Others relevant images we may want are the graphs between both trace and determinant, with respect to the concurrence. This is shown in Figure 3.3. From this image one may argue that this idea is not completely wrong, since we see that minimum trace(maximum precision) appears to be more frequent in states with small concurrence, while at the same time minimum determinant(minimum information) is achieved with higher density when the concurrence is greater.

This said, considering that every point in the image is reached by at least a state, it is clear that there is no real relationship between optimality and concurrence. Therefore we conclude that our first hypothesis is wrong.

3.1.5 *Characterization of optimal states*

Having rejected the hypothesis that factorized states are more sensible and can thus lead to better precision, we now proceed to ask if it is possible to find some

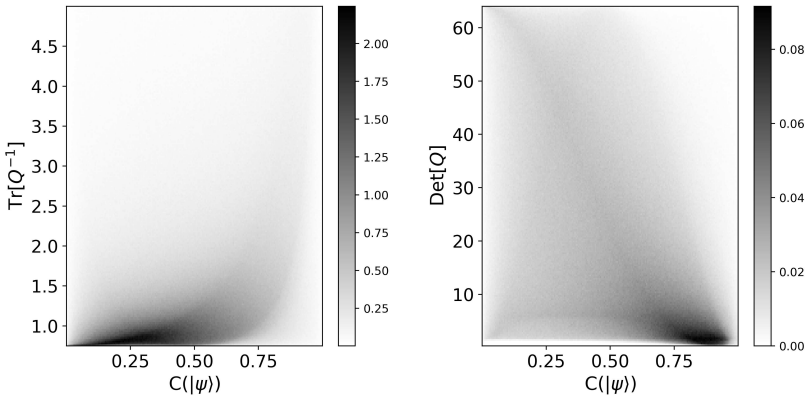

Fig. 3.3 The left column shows the relation between trace and the concurrence, while the right one between determinant and concurrence. The graphs are a density map made with 2 million points randomly generated. This shows that there is no relation between precision and information, with respect to the degree of entanglement. All points in the graph are reached by at least one state.

characteristics that give states higher sensibility to the parameters. To do this it's useful to look again at U in 1.3.3. It is not difficult seeing that it is a block matrix. We can make it more evident by rewriting it as

$$U = \begin{pmatrix} e^{-i\lambda_3}\cos(\lambda_1-\lambda_2) & -ie^{-i\lambda_3}\sin(\lambda_1-\lambda_2) & 0 & 0 \\ -ie^{-i\lambda_3}\sin(\lambda_1-\lambda_2) & e^{-i\lambda_3}\cos(\lambda_1-\lambda_2) & 0 & 0 \\ 0 & 0 & e^{i\lambda_3}\cos(\lambda_1+\lambda_2) & -ie^{i\lambda_3}\sin(\lambda_1+\lambda_2) \\ 0 & 0 & -ie^{i\lambda_3}\sin(\lambda_1+\lambda_2) & e^{i\lambda_3}\cos(\lambda_1+\lambda_2) \end{pmatrix}. \tag{3.1.12}$$

Thinking back in the canonical base, what U does is mixing the α and δ, and the β and γ components just between them. This can also be seen in Equation 3.1.2. Moreover, the two blocks in Equation 3.1.12 share the similar form

$$M = e^{i\phi}\begin{pmatrix} \cos(\theta) & -i\sin(\theta) \\ -i\sin(\theta) & \cos(\theta) \end{pmatrix}. \tag{3.1.13}$$

If we think of this as an operator acting on a qbit, we can see it represent a rotation along the x axis on the Bloch sphere. This is in fact $M = e^{i\phi}e^{-i\theta\sigma_x}$. Therefore our U acts on those($\alpha \sim \delta$ and $\beta \sim \gamma$) subspaces as a rotation. It must be noted explicitly, how these are not related to actual qbits, but just abstract ones related to the $\alpha \sim \delta$

and $\beta \sim \gamma$ pair of components.

If we now think about the most sensible states, they would be the one living on the $y - z$ plane, with $r_x = 0$. The more the state is along the plane, or similarly, the more the vector is perpendicular to the x axis, the more it rotates under U, since it acts as a rotation along the x axis.

If we follow this approach, we can actually easily generate all optimal states, taking for example the state $|0\rangle$ and rotating it along the x axis with $e^{i\theta\sigma_x}$.

$$R_x(\theta)\,|0\rangle = e^{i\theta\sigma_x}\begin{pmatrix}1\\0\end{pmatrix} = \begin{pmatrix}\cos(\theta)\\ \pm i\sin(\theta)\end{pmatrix} = \begin{pmatrix}x\\ \pm i\sqrt{1-x^2}\end{pmatrix} \tag{3.1.14}$$

Taking this for the pairs $\alpha \sim \delta$ and $\beta \sim \gamma$, by combining them we get

$$|\psi_{\text{entangled}}\rangle = \begin{pmatrix}\alpha\\ \beta e^{i\phi}\\ \pm i\sqrt{\frac{1}{2}-\beta^2}e^{i\phi}\\ \pm i\sqrt{\frac{1}{2}-\alpha^2}\end{pmatrix}, \tag{3.1.15}$$

which we recognize to be exactly 3.1.10.

3.1.6 *Optimization at fixed trace*

Looking back at Figure 3.1 what we have found is the most top-left point. Now we want to describe all the top curve, so all states maximizing the determinant at any given trace. Formally, what we want to do is maximize the determinant function, keeping the trace as a constraint.

To do this we will require the gradient of the determinant to be 0, and also change a variable into the trace through the trace expression. Let's start with removing a trivial degree of freedom, by imposing that the coefficients are

normalized($\delta = \sqrt{1-\alpha^2-\beta^2-\gamma^2}$). We get

$$\begin{aligned}\text{Det}[Q] = 1024\Big[\beta^4 - 2\beta^2\gamma^2\cos\left(2(\phi_\beta-\phi_\gamma)\right)+\gamma^4\Big]\Big[-2\delta^2\left[-\beta^2-\gamma^2-\delta^2+1\right]\cos\left(2\phi_\delta\right)\\ +\left[-\beta^2-\gamma^2-\delta^2+1\right]^2+\delta^4\Big].\end{aligned} \tag{3.1.16}$$

Then by imposing $\text{Tr}[Q^{-1}] \equiv t$, and expliciting it for α we get a function $\alpha = \alpha(\beta, \gamma, \phi_\beta - \phi_\gamma, \phi_\delta, t)$, given by

$$\alpha = \frac{1}{2}\sqrt{2\left(1-\beta^2-\gamma^2\right) \pm \frac{\sqrt{2}\sec^2\left(\phi_\delta\right)\sqrt{f(\beta,\gamma,\phi_\beta-\phi_\gamma,\phi_\delta,t)}}{-3\beta^2-32\beta^2\gamma^2t\cos\left(2(\phi_\beta-\phi_\gamma)\right)-3\gamma^2+16\beta^4t+16\gamma^4t}} \tag{3.1.17}$$

with

$$\begin{aligned}f = &\left[\beta^2+\gamma^2-1\right]\cos^2\left(\phi_\delta\right)\left[-3\beta^2-32\beta^2\gamma^2t\cos\left(2(\phi_\beta-\phi_\gamma)\right)-3\gamma^2+16\beta^4t+16\gamma^4t\right]\\ &\Big[\left[\beta^2+\gamma^2-1\right]\cos\left(2\phi_\delta\right)\left[-3\beta^2-32\beta^2\gamma^2t\cos\left(2(\phi_\beta-\phi_\gamma)\right)-3\gamma^2+16\beta^4t+16\gamma^4t\right]\\ &+4\beta^2\gamma^2\cos\left(2(\phi_\beta-\phi_\gamma)\right)\left[8t\left(\beta^2+\gamma^2-1\right)+3\right]-3\gamma^2-16\beta^6t\\ &+\beta^4\left[-16\left(\gamma^2-1\right)t-3\right]+\beta^2\left[6\gamma^2-16\gamma^4t-3\right]+\gamma^4\left[-16\left(\gamma^2-1\right)t-3\right]\Big].\end{aligned} \tag{3.1.18}$$

Where the $\pm$ in Equation 3.1.17 is due to the symmetry in $\alpha \sim \delta$, and so we can choose either of the two getting the same result. Putting it in Equation 3.1.16 we get

$$\text{Det}[Q] = -\frac{3072\left[\beta^2+\gamma^2-1\right]\left[\beta^4-2\beta^2\gamma^2\cos\left(2\left(\phi_\beta-\phi_\gamma\right)\right)+\gamma^4\right]^2}{-3\beta^2-3\gamma^2+16\beta^4t-32\beta^2\gamma^2t\cos\left(2\left(\phi_\beta-\phi_\gamma\right)\right)+16\gamma^4t}. \tag{3.1.19}$$

By doing so we have reduced the free parameters to $\text{Det}[Q] = \text{Det}[Q](\beta, \gamma, \phi_\beta - \phi_\gamma, t)$. At this point we could continue looking for maxima, but one must be careful. In fact there could exists choices of parameters such that

$$\exists\ \alpha, \delta, \phi_\delta\ :\nexists\ \beta, \gamma, \phi_\beta - \phi_\gamma, t\ :\ \text{Tr}[Q^{-1}] = t. \tag{3.1.20}$$

This follows from the fact that the argument of the square roots of Equation 3.1.17 could be negative, but α must be real. In general this condition is non trivial, and this problem will be addressed and solved with a different approach in Section 3.2.

Despite this we can extract some solutions quite easily by restraining the domain. By plotting points in the Trace-Determinant plane as in Figure 3.1, it can be seen that if we arbitrarily impose either $\gamma = 0$ or $\beta = 0$, the set of point reached is the same. The same is true if we impose also $\phi_\delta = 0$. This means that (some) optimal states are still achievable despite our restrictions. For the sake of simplification we thus say that $\gamma = 0$ and $\phi_\delta = 0$. An advantage of this case is that the domain of α in the $\phi_\beta - \phi_\gamma \sim \beta$ plane is a rectangle, with width dependent on t, as shown in Figure 3.4

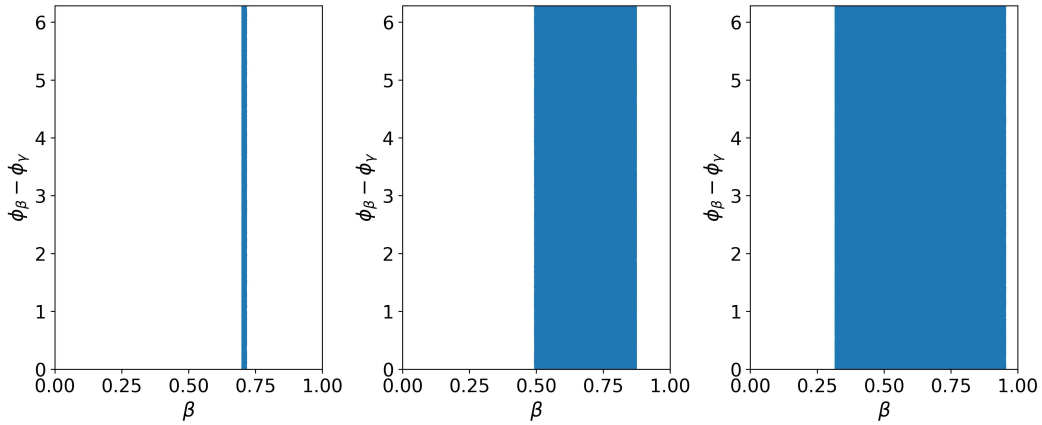

Fig. 3.4 The three graphs represent the domains of α in the $\beta \sim \phi_\beta - \phi_\gamma$ plane. The leftmost panel is evaluated for $t = 0.76$, the center one at $t = 1$ and the rightmost at $t = 2$.

Under these assumptions the determinant becomes

$$\mathrm{Det}[Q] = -\frac{3072\beta^6\left(\beta^2-1\right)}{16\beta^2 t - 3}, \tag{3.1.21}$$

which is maximized in

$$\beta(t) = \frac{\sqrt{\frac{\sqrt{64t^2-60t+9}+8t+3}{t}}}{2\sqrt{6}}. \tag{3.1.22}$$

To be sure the solution is valid we now must check wether it lies in the domain, for every t. This is shown to be the case in Figure 3.5, where we see how this value is always within the right and left boundary of the domain at any given t.

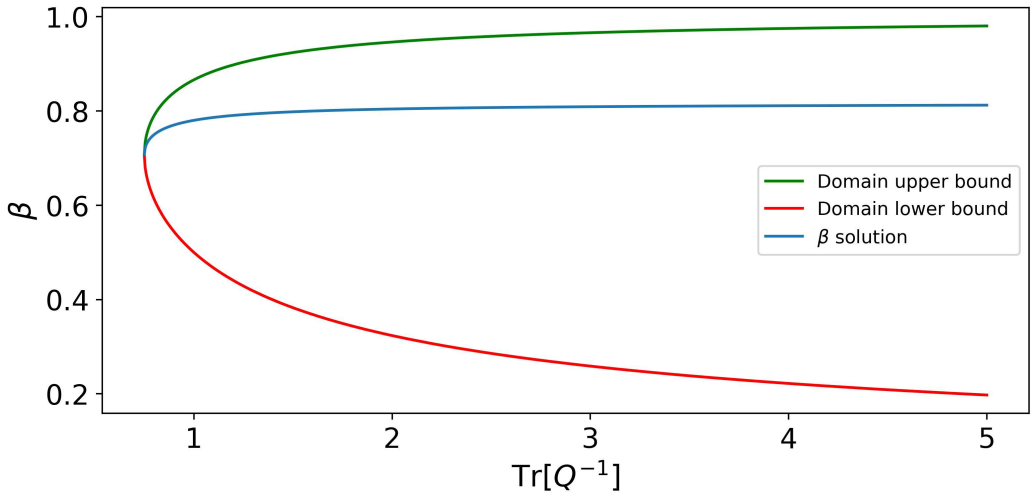

Fig. 3.5 The graph shows how for every $t \in [\frac{3}{4}, +\infty)$ the β is inside the domain range. This means that the formula is a valid solution for every t. The graphs shows only values up to $\mathrm{Tr}[Q^{-1}] = 5$, but by plotting on larger domains it can be seen that the asymptotic values are already been almost reached.

Therefore, putting everything together we have that the solution is

$$|\psi\rangle = \begin{pmatrix} \alpha(\beta, \gamma, \phi_\beta - \phi_\gamma, \phi_\delta, t) \\ \beta(t) e^{i\phi} \\ 0 \\ \sqrt{1 - \alpha^2 - \beta^2} \end{pmatrix} \tag{3.1.23}$$

with $\alpha(\beta, \gamma, \phi_\beta, \phi_\gamma, \phi_\delta, t)$ given by Equation 3.1.17 and $\beta(t)$ by Equation 3.1.22. Due to symmetries other solutions are obtainable by swapping $\alpha \leftrightarrow \delta$ and/or $\beta \leftrightarrow \gamma$.

Solutions with different conditions present much harder domains. Therefore to avoid unnecessary complications, a different approach is presented, that will also be able to find all possible solutions in a concise way.

3.2 OPTIMIZATION IN THE BELL BASIS PARAMETRIZATION

As it has been pointed out in Section 1.3.1 the Bell basis is the one that diagonalizes U. What we will see is that expressing quantities through the natural parametrization in this base, will also lead us to simpler and more symmetrical quantities, and

solutions.

3.2.1 *Relevant quantities*

For convenience let's rewrite the U in the Bell basis

$$U = \begin{pmatrix} e^{-i(\lambda_1-\lambda_2+\lambda_3)} & 0 & 0 & 0 \\ 0 & e^{-i(\lambda_1+\lambda_2-\lambda_3)} & 0 & 0 \\ 0 & 0 & e^{i(\lambda_1-\lambda_2-\lambda_3)} & 0 \\ 0 & 0 & 0 & e^{i(\lambda_1+\lambda_2+\lambda_3)} \end{pmatrix}_B . \tag{3.2.1}$$

From now on in this section objects will be implicitly assumed to be in the Bell basis, therefore subscripts regarding the base will be dropped. Additionally latin letters will be used to parametrize the states, in order to distinguish them from the canonical ones.

In a similar way to what we've done in the canonical base, we start from parametrizing in a natural way the initial state vector, as

$$|\psi_0\rangle \equiv \begin{pmatrix} a \\ be^{i\phi_b} \\ ce^{i\phi_c} \\ de^{i\phi_d} \end{pmatrix}. \tag{3.2.2}$$

We then evolve it with U, getting

$$|\psi_{\underline{\lambda}}\rangle = \begin{pmatrix} ae^{-i(\lambda_1-\lambda_2+\lambda_3)} \\ be^{i(\phi_b-\lambda_1-\lambda_2+\lambda_3)} \\ ce^{i(\phi_c+\lambda_1-\lambda_2-\lambda_3)} \\ de^{i(\phi_d+\lambda_1+\lambda_2+\lambda_3)} \end{pmatrix}. \tag{3.2.3}$$

From this we can calculate the QFI with Equation 2.1.7, which is

$$Q = \begin{pmatrix} Q_{11} & Q_{12} & Q_{13} \\ Q_{21} & Q_{22} & Q_{23} \\ Q_{31} & Q_{32} & Q_{33} \end{pmatrix} \tag{3.2.4}$$

with

$$\begin{aligned}
Q_{11} &= -16\left(b^2+d^2-1\right)\left(b^2+d^2\right)\\
Q_{22} &= -16\left(b^2+c^2-1\right)\left(b^2+c^2\right)\\
Q_{33} &= -16\left(c^2+d^2-1\right)\left(c^2+d^2\right)\\
Q_{12} &= Q_{21} = 16\left(b^4+b^2\left(c^2+d^2-1\right)+c^2d^2\right)\\
Q_{13} &= Q_{31} = 16\left(d^2-\left(b^2+d^2\right)\left(c^2+d^2\right)\right)\\
Q_{23} &= Q_{32} = 16\left(c^2\left(b^2+d^2-1\right)+b^2d^2+c^4\right)
\end{aligned} \tag{3.2.5}$$

An interesting thing to note is that there is no dependence on the angles. This fact automatically reduces the domain space of optimization, to just 3 dimensions(b, c, d). Solutions will then be defined up to relative phases applicable at the end.

In particular the normalization condition $a^2+b^2+c^2+d^2=1$ has been already applied to Equation 3.2.5, removing the apparent degree of freedom of a. Without this the QFI is slightly more symmetrical, but have longer components. Since this won't be used, the shorter expressions have been provided. The trace of its inverse, and the determinant of the QFI are

$$\mathrm{Tr}[Q^{-1}] = \frac{3}{64}\left(\frac{1}{a^2}+\frac{1}{b^2}+\frac{1}{c^2}+\frac{1}{d^2}\right) = \frac{3}{64}\left(\frac{1}{b^2}+\frac{1}{c^2}+\frac{1}{d^2}+\frac{1}{1-b^2-c^2-d^2}\right), \tag{3.2.6}$$

$$\mathrm{Det}[Q] = 16384a^2b^2c^2d^2 = 16384\left(1-b^2-c^2-d^2\right)^2b^2c^2d^2. \tag{3.2.7}$$

3.2.2 *Optimal states in the Bell parametrization*

To find optimal states we minimize the trace. We can do so by imposing its gradient to be 0, and explicit the constraint with respect to a parameter. Starting with d we have

$$\partial_d\mathrm{Tr}[Q^{-1}] = 0 \Rightarrow d = \frac{\sqrt{3}\left(1-b^2-c^2\right)}{\sqrt{-6b^2-6c^2+6}} \Rightarrow \mathrm{Tr}[Q^{-1}] = \frac{3}{64}\left(\frac{1}{b^2}+\frac{1}{c^2}+\frac{4}{1-b^2-c^2}\right). \tag{3.2.8}$$

Following up with c we have

$$\partial_c\mathrm{Tr}[Q^{-1}] = 0 \Rightarrow c = \sqrt{\frac{1-b^2}{3}} \Rightarrow \mathrm{Tr}[Q^{-1}] = \frac{24b^2+3}{64b^2-64b^4}. \tag{3.2.9}$$

And lastly the b is

$$\partial_b \mathrm{Tr}[Q^{-1}] = 0 \Rightarrow b = \frac{1}{2} \Rightarrow c = \frac{1}{2} \wedge d = \frac{1}{2} \Rightarrow \mathrm{Tr}[Q^{-1}] = \frac{3}{4}. \tag{3.2.10}$$

Putting together the conditions we can see that optimal states have the form

$$|\psi_{\text{optimal}}\rangle = \begin{pmatrix} \frac{1}{2} \\ \frac{1}{2}e^{i\phi_\beta} \\ \frac{1}{2}e^{i\phi_\gamma} \\ \frac{1}{2}e^{i\phi_\delta} \end{pmatrix}. \tag{3.2.11}$$

3.2.3 *Optimization at fixed trace*

We can now restore to where we stopped in Section 3.1.6. As before, what we want to do is maximize the determinant, substituting the trace as a parameter. Starting with the normalization constraint we have

$$\mathrm{Det}[Q] = 16384\,(1 - b^2 - c^2 - d^2)\,b^2c^2d^2. \tag{3.2.12}$$

By calling $\mathrm{Tr}[Q^{-1}] \equiv t$ and expliciting for d we get

$$d = \sqrt{\frac{1 - c^2 - b^2 \pm \frac{\sqrt{[b^2+c^2-1][64b^2c^2t(b^2+c^2-1)-3(b^4-b^2(2c^2+1)+c^4)+3c^2][b^2(64c^2t-3)-3c^2]}}{b^2(64c^2t-3)-3c^2}}{2}}, \tag{3.2.13}$$

where we can choose either $\pm$, due to the symmetry between $a \sim d$. Replacing either of the two in the determinant we get

$$\mathrm{Det}[Q] = \frac{49152b^4c^4\,(1 - b^2 - c^2)}{b^2\,(64c^2t - 3) - 3c^2}. \tag{3.2.14}$$

If we now plot this determinant in function of b, c, at fixed t, keeping in mind the restricted domain imposed by Equation 3.2.13, we get Figure 3.6.

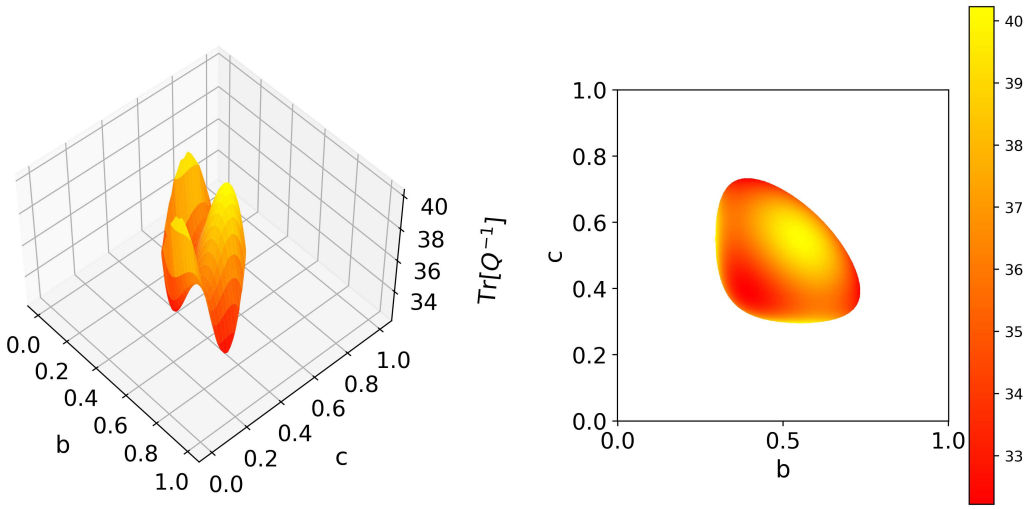

Fig. 3.6 Determinant in function of b and c, respectively on the x and y axis. Parameter t is set to 1. The left panel shows the 3D visualization, while the right panel is the relative 2D heatmap.

What we can see is that there are 3 maxima, one on the bisector, and the other two on the same x or y as the center one, but on a side of the border. It can be proven that those 3 points have the same determinant. Additionally for every t the function has a similar form to the one presented, and these 3 characteristic maxima are always present. We can for example look for the one on the bisector, imposing $b = c$. At this point we can derive the determinant with respect to b, getting

$$\partial_b(\mathrm{Tr}[Q^{-1}]\Big|_{b=c}) = \partial_b \frac{24576b^6\,(1-2b^2)}{32b^2t-3} = -\frac{49152b^5\,(192b^4t-8b^2(8t+3)+9)}{(3-32b^2t)^2}. \tag{3.2.15}$$

By imposing this to 0 we get that b is

$$b = \frac{\sqrt{\frac{\pm\sqrt{64t^2-60t+9}+8t+3}{t}}}{4\sqrt{3}}, \tag{3.2.16}$$

where the degeneracy is due to having a minima and a maxima. By comparing the determinants in the two cases we can see that the + gives the maximum, and the − the minimum. We call $s_1 \equiv b_+$ the solution with the +. The final expression of the

determinant using s_1 becomes

$$\mathrm{Det}[Q](t) = \frac{\left(-\sqrt{64t^2-60t+9}+16t-3\right)\left(\sqrt{64t^2-60t+9}+8t+3\right)^3}{36t^4\left(2\sqrt{64t^2-60t+9}+16t-3\right)}, \tag{3.2.17}$$

which is the maximum determinant achievable at trace t.

Now that we found b and c($b = c$ given from Equation 3.2.16) we can plug back this into a and d, from which we get that one of either a or d is equal to b, while the other is

$$a = \frac{1}{4}\sqrt{\frac{\sqrt{64t^2-60t+9}+8t-3}{t}} \equiv s_2. \tag{3.2.18}$$

Similarly, the point on the border would have given that either b or c where this fourth different value s_2, and the other three all given by Equation 3.2.16.

In conclusion the suboptimal states are given by

$$|\psi_{\text{suboptimal}}\rangle = \begin{pmatrix} s_2 \\ s_1 e^{i\phi_b} \\ s_1 e^{i\phi_c} \\ s_1 e^{i\phi_d} \end{pmatrix}, \tag{3.2.19}$$

where s_2 can be switched in either of the four components.

3.3 ROBUSTNESS AGAINST NOISE

Having found many optimal states, we now want to characterize their robustness against noisy channels.

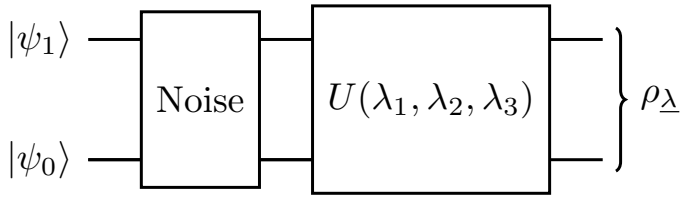

Fig. 3.7 Quantum circuit representing how noisy channel alter the prepared probe states before performing the U evolution.

The circuit we will consider is the one presented in Figure 3.7. We assume that after the preparation of our states, they can undergo some generic noise before entering the entangling gate. At this level we restrain ourselves from overclassifying states under specific noises, since they may be specific of the given implementation of the system. Instead we want to describe qualitatively the goodness and robustness of the solutions found. To do this we will apply some simple noises, and see how optimal precision change. To avoid excessive descriptiveness, three interesting class of states have been handpicked to show how various states are affected by noise. These classes are the following

$$
\begin{aligned}
|\psi_1\rangle &\equiv \begin{pmatrix} \frac{1}{\sqrt{2}} \\ \frac{1}{\sqrt{2}} e^{i\phi} \\ 0 \\ 0 \end{pmatrix} = |0\rangle \otimes \begin{pmatrix} \frac{1}{\sqrt{2}} \\ \frac{1}{\sqrt{2}} e^{i\phi} \end{pmatrix} \\
|\psi_2\rangle &\equiv \begin{pmatrix} \frac{1}{\sqrt{2}} \\ 0 \\ \frac{1}{\sqrt{2}} e^{i\phi} \\ 0 \end{pmatrix} = \begin{pmatrix} \frac{1}{\sqrt{2}} \\ \frac{1}{\sqrt{2}} e^{i\phi} \end{pmatrix} \otimes |0\rangle \\
|\psi_3\rangle &\equiv \begin{pmatrix} 0.3 \\ 0.2\, e^{i\phi} \\ i\sqrt{\frac{1}{2} - 0.2^2} e^{i\phi} \\ i\sqrt{\frac{1}{2} - 0.3^2} \end{pmatrix}.
\end{aligned}
\tag{3.3.1}
$$

3.3.1 *General procedure*

Using the quantum circuit description, and quantum maps, as described in Sections 1.2.3 and 1.1.2 respectively, we can immediately write the final statistical operator of the circuit described in Figure 3.7 as

$$
\rho_{\underline{\lambda}} = (1-p) U \rho_0 U^\dagger + p U E \rho_0 E^\dagger U^\dagger, \tag{3.3.2}
$$

with E the evolution describing the noise, ρ_0 the initial statistical operator, and p the probability of the noise occurring. This will be the statistical operator used to compute the $\mathrm{Tr}[Q^{-1}]$.

Since we can in general assume that p is small, we will see only noise acting on one of the two qbits(i.e. the second). Also, we do this to avoid unnecessary details as mentioned before. The noises that will be analyzed are the bit flip, the phase flip, the bit phase flip, the decoherence and the depolarizing channel.

The introduction of noises complicates the computation. In fact it is no longer possible to calculate the QFI via Equation 2.1.7, since the noise creates a statistical model that is not pure. Instead we have to rely on the more general version provided by Equation 2.1.6. Despite this being technically solvable analytically, due to the high complexity a numerical approach has been implemented instead. In particular given a statistical model, parametrized by p and ϕ, we use Equation 2.1.6 to calculate the QFI, and then evaluate $\mathrm{Tr}[Q^{-1}]$.

The goal is to see if by varying the probe states over ϕ, there are certain values that are insensible to the rumor. Also, where the noise modify the precision, we want to see if this is rapidly changing, or it is given by a convex curve(which would be ideal).

3.3.2 *Robustness against the noise*

The first three noises to be examined are the bit-flip, the bit-phase-flip and the phase-flip. These are respectively given by

$$\begin{aligned} E_{BF} &\equiv \sigma_x \otimes \equiv \sigma_x^{(1)} \\ E_{BPF} &\equiv \sigma_y \otimes \mathbb{1} \equiv \sigma_y^{(1)} \\ E_{PF} &\equiv \sigma_z \otimes \mathbb{1} \equiv \sigma_z^{(1)}. \end{aligned} \tag{3.3.3}$$

If we now compute the trace of the inverse QFI, using the state given by Equation 3.3.2, with E the noise being analyzed, applied with probability p, we get the graphs of Figure 3.8, 3.10 and 3.9. Each one shows the precision in function of p and ϕ. As already mentioned, for each type of noise we see how the 3 classes of states defined in Equation 3.3.1 perform.

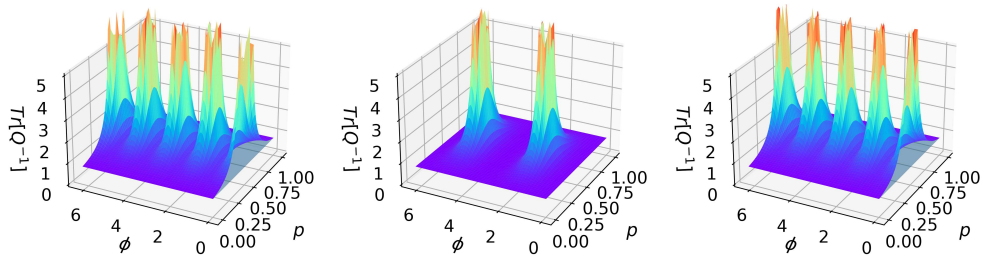

Fig. 3.8 Graphs that shows the relation between precision(z axis), at a given probability of the noise occurring(x axis), with a probe state with ϕ(y axis). The type of noise analyzed here is the bit-flip. The three panels corresponds to the three classes of states described in 3.3.1

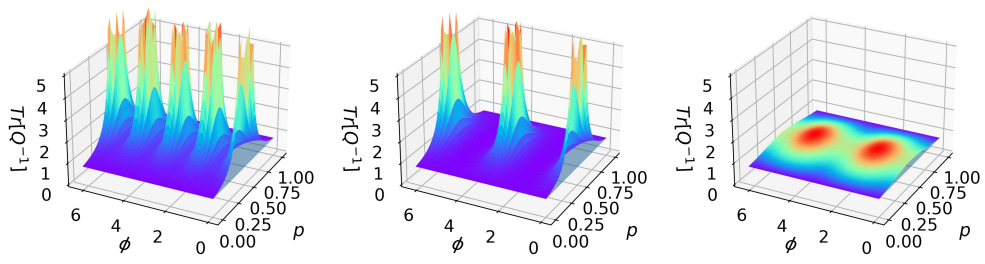

Fig. 3.9 Graphs that shows the relation between precision(z axis), at a given probability of the noise occurring(x axis), with a probe state with ϕ(y axis). The type of noise analyzed here is the bit-phase-flip. The three panels corresponds to the three classes of states described in 3.3.1

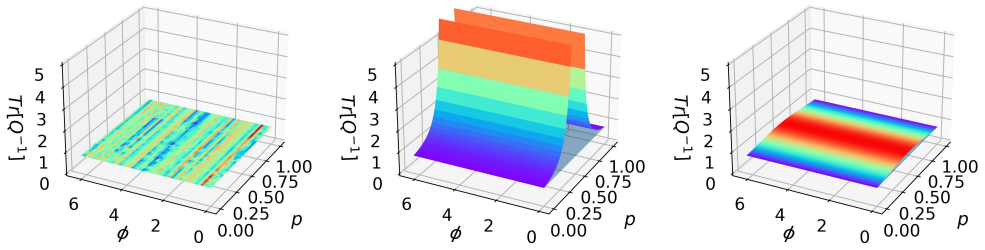

Fig. 3.10 Graphs that shows the relation between precision(z axis), at a given probability of the noise occurring(x axis), with a probe state with ϕ(y axis). The type of noise analyzed here is the phase-flip. The three panels corresponds to the three classes of states described in 3.3.1

Following up, the decoherence can be described for example with projectors onto the $|0\rangle$ and $|1\rangle$ states(always referred just to the first qbit). This can be written with

$$\rho_{\underline{\lambda}} = (1-p)U\rho_0 U^\dagger + \frac{p}{2}U(|0\rangle\langle 0|\otimes\mathbb{1})\rho_0(|0\rangle\langle 0|\otimes\mathbb{1})U^\dagger + \frac{p}{2}U(|1\rangle\langle 1|\otimes\mathbb{1})\rho_0(|1\rangle\langle 1|\otimes\mathbb{1})U^\dagger. \tag{3.3.4}$$

Its graphs of $\mathrm{Tr}[Q^{-1}]$ are shown in Figure 3.11.

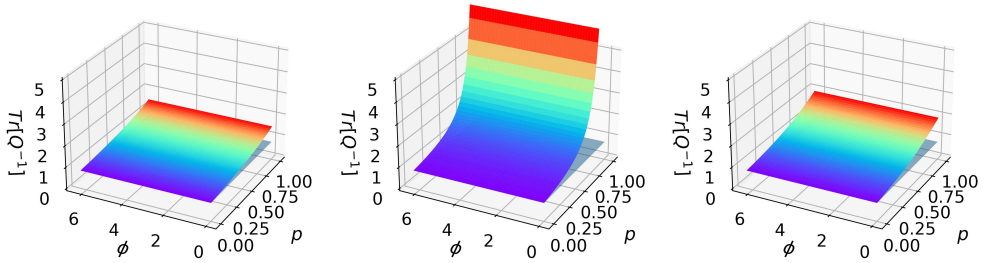

Fig. 3.11 Graphs that shows the relation between precision(z axis), at a given probability of the noise occurring(x axis), with a probe state with ϕ(y axis). The type of noise analyzed here is the decoherence. The three panels corresponds to the three classes of states described in 3.3.1

Lastly we have the depolarizing channel. This channel in particular is interesting since it is a combination of the first three noises, with equal probability. For this

reason it gives us a more generic indication of the general sensibility to generic noise. It is described by

$$\rho_{\underline{\lambda}} = (1-p)U\rho_0 U^\dagger + \frac{p}{3}\sum_{k\in\{x,y,z\}} U\sigma_k^{(1)}\rho_0\sigma_k^{(1)}U^\dagger. \tag{3.3.5}$$

Its graphs of $\mathrm{Tr}[Q^{-1}]$ are in Figure 3.12.

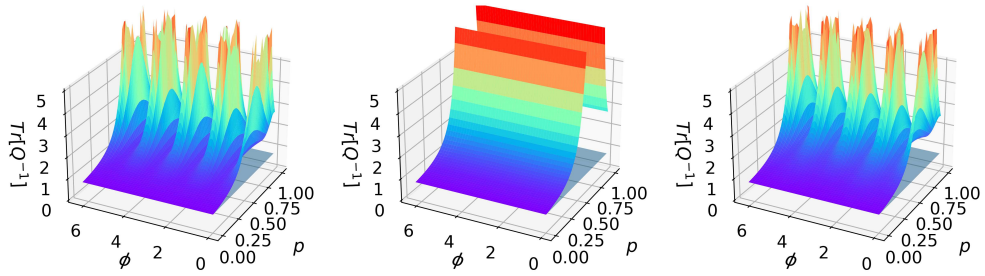

Fig. 3.12 Graphs that shows the relation between precision(z axis), at a given probability of the noise occurring(x axis), with a probe state with ϕ(y axis). The type of noise analyzed here is the depolarizing channel. The three panels corresponds to the three classes of states described in 3.3.1

3.3.3 *Noise analysis*

What we can see from the graphs is that despite being optimal states, they present different sensibility to noise. In particular, we can see two important facts. The first is that in all cases, for $p <<$ the function is convex. Thus, robustness is ensured for low noise and we don't have no-go theorems. The second remark is that we can see that for every type of noise there are phases, such that precision remains relatively small. In particular the phases $\phi = \frac{\pi}{4} + n\frac{\pi}{2}$ in state $|\psi_1\rangle$ or $|\psi_3\rangle$ have precision that is always smaller than 2.

3.4 SUBOPTIMAL MEASURES

Concluding, we address the last objective of the thesis that is the determination of suboptimal measurements. In fact, despite having optimal measures described by

the SLDs, we may want a more easily implementable unique measure, that is able to approximate optimal precision for all three parameters. In particular, we will consider local spin measurements on each qbit. The directions in which the two spins are measured can be different, and will be denoted by $\underline{n}_1$ and $\underline{n}_2$. The spin measure can be thus described as

$$M(\underline{n}_1, \underline{n}_2) = (\underline{n}_1 \cdot \underline{P}) \otimes (\underline{n}_2 \cdot \underline{P}), \tag{3.4.1}$$

with $\underline{P} \equiv \{\sigma_x, \sigma_y, \sigma_z\}$ the vector of Pauli matrices.

3.4.1 *SLDs with an optimal probe*

Before looking into suboptimal measures let's show the form of optimal SLDs. We can calculate them using Equation 2.1.3, with $\rho_{\underline{\lambda}}$ obtained with the state described in Equation 3.1.2. The expression obtained this way is generally involved. A possible simplification we can do is see the SLDs in the case of optimal probes. For example we can consider the probe given by the first element of Equation 3.1.9. Additionally, a useful basis onto which expressing the matrices is the one provided by

$$\tilde{M} = \sum_{j,k\in\{0,1,2,3\}} \mathrm{Tr}[(\sigma_j \otimes \sigma_k)M] \tag{3.4.2}$$

The advantage of this basis is that it is straightforward understanding the spin direction from the matrix form. By doing this we get

$$
\begin{aligned}
L_1 &= \\
&-4\begin{pmatrix} 0 & 0 & \sin(2\lambda_1)\sin(\xi) & -\sin(2\lambda_2)\cos(2\lambda_1) \\ 0 & 0 & \sin(2\lambda_1)\sin(2\lambda_2) & -\cos(2\lambda_1)\sin(\xi) \\ \cos(2\lambda_1)\cos(\xi) & \cos(2\lambda_1)\cos(2\lambda_2) & 0 & 0 \\ \sin(2\lambda_1)\cos(2\lambda_2) & \sin(2\lambda_1)\cos(\xi) & 0 & 0 \end{pmatrix} \\
L_2 &= \\
&4\begin{pmatrix} 0 & -\sin(2\lambda_2)\cos(\xi) & 0 & \sin(2\lambda_1)\cos(2\lambda_2) \\ \cos(2\lambda_2)\sin(\xi) & 0 & \cos(2\lambda_1)\cos(2\lambda_2) & 0 \\ 0 & \sin(2\lambda_1)\sin(2\lambda_2) & 0 & -\cos(2\lambda_2)\cos(\xi) \\ -\sin(2\lambda_2)\cos(2\lambda_1) & 0 & -\sin(2\lambda_2)\sin(\xi) & 0 \end{pmatrix} \\
L_3 &= 4\begin{pmatrix} 0 & -\cos(2\lambda_2)\sin(\xi) & \cos(2\lambda_1)\cos(\xi) & 0 \\ \sin(2\lambda_2)\cos(\xi) & 0 & 0 & \sin(2\lambda_1)\cos(\xi) \\ \sin(2\lambda_1)\sin(\xi) & 0 & 0 & \sin(2\lambda_2)\sin(\xi) \\ 0 & -\cos(2\lambda_1)\sin(\xi) & \cos(2\lambda_2)\cos(\xi) & 0 \end{pmatrix}
\end{aligned}
\tag{3.4.3}
$$

with $\xi \equiv 2\lambda_3 + \phi$. In the case of $\underline{\lambda} = \underline{0}$ this reduces to

$$
\begin{aligned}
L_1 &= \begin{pmatrix} 0 & 0 & 0 & 0 \\ 0 & 0 & 0 & 4\sin(\phi) \\ -4\cos(\phi) & -4 & 0 & 0 \\ 0 & 0 & 0 & 0 \end{pmatrix} \\
L_2 &= \begin{pmatrix} 0 & 0 & 0 & 0 \\ 4\sin(\phi) & 0 & 4 & 0 \\ 0 & 0 & 0 & -4\cos(\phi) \\ 0 & 0 & 0 & 0 \end{pmatrix} \\
L_3 &= \begin{pmatrix} 0 & -4\sin(\phi) & 4\cos(\phi) & 0 \\ 0 & 0 & 0 & 0 \\ 0 & 0 & 0 & 0 \\ 0 & -4\sin(\phi) & 4\cos(\phi) & 0 \end{pmatrix}.
\end{aligned}
\tag{3.4.4}
$$

What this tells us, is that in the limit of $\underline{\lambda} = \underline{0}$, the three SLDs are

$$\begin{aligned} L_1 &= -4\sigma_2 \otimes (\sigma_0 + \sigma_1) \\ L_2 &= 4\sigma_1 \otimes (\sigma_0 + \sigma_2) \\ L_3 &= 4(\sigma_0 + \sigma_4) \otimes \sigma_2 \end{aligned} \tag{3.4.5}$$

with a suitable choice of ϕ. Clearly these results are very specific on both the probe states, and especially on the choice of $\underline{\lambda}$.

3.4.2 *Spin measures*

We now want to see if there is a good choice of $\underline{n}_1$ and $\underline{n}_2$, such that for every $\underline{\lambda}$ the precision is low. The way this has been done is by numerically evaluating $\mathrm{Tr}[F^{-1}]$, using the definition of the Fisher information provided in Equation 2.1.4. In particular, considering the measure described by Equation 3.4.1, the x we're measuring are the two "up" or "down" spins along the specific axes. Therefore with

$$p(s_1, s_2|\underline{\lambda}) = |(\langle s_1| \otimes \langle s_2|)U|\psi_0\rangle|^2, \tag{3.4.6}$$

we get

$$F_{jk} = \sum_{s_1, s_2 \in \{\pm 1\}} \frac{\partial_j p(s_1, s_2|\underline{\lambda})\, \partial_k p(s_1, s_2|\underline{\lambda})}{p(s_1, s_2|\underline{\lambda})}. \tag{3.4.7}$$

Now the crucial part is the optimization process. The main problem is that it appears that there is no single measure, with a fixed probe, able to have a small $\mathrm{Tr}[F^{-1}]$ for all possible values of $\underline{\lambda}$. Under this observation, what can be empirically showed to be a solution is trying to perform measures with some different probes. The experimental approach can be described as follows:

1. Select a measure $M(\underline{n}_1, \underline{n}_2)$.
2. Select a set of probe states.
3. Perform a statistics on each probe state separately. For each set of data we have that the sum of the variances is given by $\mathrm{Tr}[F^{-1}]$, using the F described in Equation 3.4.7.
4. Out of the four sets of data the one with minimum $\mathrm{Tr}[F^{-1}]$ is selected.

A small practical variation of this could be accounting for every set of measures, but weighting them by their respective estimated variances. This way we would also use the information obtained through the non optimal measures needed to determine the state in our chosen probes set with minimum variance. Then, of course in a practical environment as soon as it can be determined which probe has minimum $\mathrm{Tr}[F^{-1}]$, one would do all the measures with just that state.

It must be noted that the way variance is calculated for angles differs from the way it is usually done. In fact angles live in a domain that is periodic. The correct way is through the Holevo variance, defined as

$$V_H(\hat{\theta}) \equiv \mu^{-2} - 1, \tag{3.4.8}$$

with

$$\mu \equiv |E(e^{i\hat{\theta}})| = \int_0^{2\pi} e^{i\phi} p(\phi) d\phi, \tag{3.4.9}$$

with $p(\theta)$ the distribution over the angles.

Let's now discuss the optimization of the measure. We will examine the case where four possible input states have been selected. These are the states described in Equation 3.1.9, by imposing $\phi = 0$. It must be mentioned that these states have been selected due to their simplicity, and not due to some specific characteristic. What we now do is:

1. Select a random measure $M(\underline{n}_1, \underline{n}_2)$.
2. Uniformly generate a random list of N $\underline{\lambda}$.
3. For every $\underline{\lambda}$ calculate $\mathrm{Tr}[F^{-1}]$ for each of the four states.
4. For every $\underline{\lambda}$ consider only the minimum of the four variances($\mathrm{Tr}[F^{-1}]$).

Proceeding this way, we end up with a list of N variances, being the minimum of the four for each $\underline{\lambda}$. Out of these, it is interesting to look for two specific quantities: the average precision, and the max $\mathrm{Tr}[F^{-1}]$(worst case). In this way we can optimize the best measure on those values. In Figure 3.13 we can see that the average precision is comparable to the optimal, being around $\mathrm{Tr}[F^{-1}] = 5$, with a best of $\mathrm{Tr}[F^{-1}] \approx 2$.

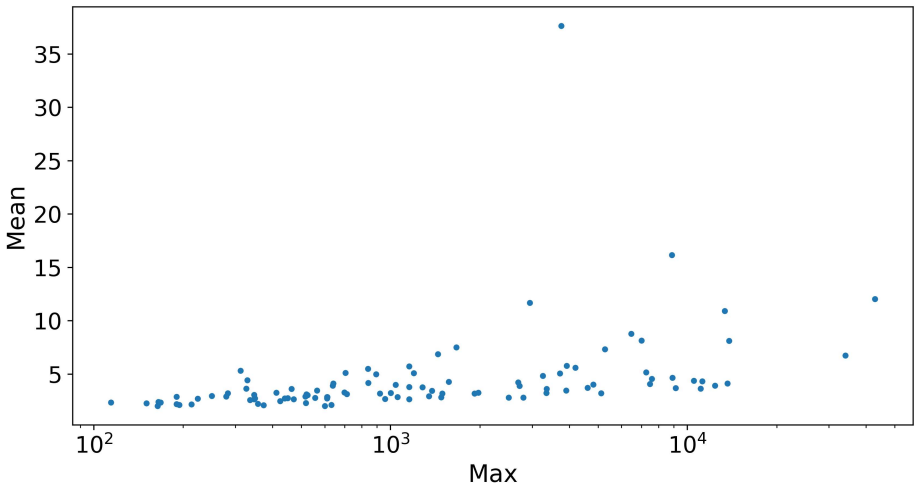

Fig. 3.13 Each point in the graph corresponds to a different measure $M(\underline{n}_1, \underline{n}_2)$. The coordinates of each point are the maximum $\mathrm{Tr}[F^{-1}]$, and the average $\mathrm{Tr}[F^{-1}]$ obtained through the procedure described in the text. Each point has been generated accounting for 10'000 values of $\underline{\lambda}$ generated uniformly, and using the 4 probes mentioned in the text.

On the contrary, the max value ranges from $\mathrm{Tr}[F^{-1}] \approx 100$ up to $\mathrm{Tr}[F^{-1}] \approx 40'000$. What this tells us is that despite using multiple states, there are still values of $\underline{\lambda}$ for which neither of the four allows a good estimate. This will be addressed later by seeing if this can be resolved by increasing the number of probes, or there are certain $\underline{\lambda}$ intrinsically bad, for which every probe will lead to a big value of $\mathrm{Tr}[F^{-1}]$.

Another interesting graph to consider is the following. In Figure 3.14 it is showed the $\mathrm{Tr}[F^{-1}]$ distribution, sampling over the possible $\underline{\lambda}$. To do this, the measure used is the leftmost point in Figure 3.13. This measure in simple precision is described by

$$\underline{n}_1 = \begin{pmatrix} 0.97174852 \\ 0.20283044 \\ 0.12068401 \end{pmatrix}, \quad \underline{n}_2 = \begin{pmatrix} 0.01780627 \\ 0.57226754 \\ 0.81987365 \end{pmatrix}. \tag{3.4.10}$$

From this graph we can reconcile the fact that despite having such large maximum values, the average is still very small. This is in fact due to the fact that the probability of getting a given variance decays almost exponentially with its value.

Using again the measure described in Equation 3.4.10, we can check our hypothesis that with a greater number of probes we can reduce the maximum $\mathrm{Tr}[F^{-1}]$. To allow for a greater choice of optimal probes we now use the one described in Equation 3.1.10, where 100 random $a, b \in [0, \frac{1}{\sqrt{2}}]$ and $\phi \in [0, 2\pi)$ has been chosen.

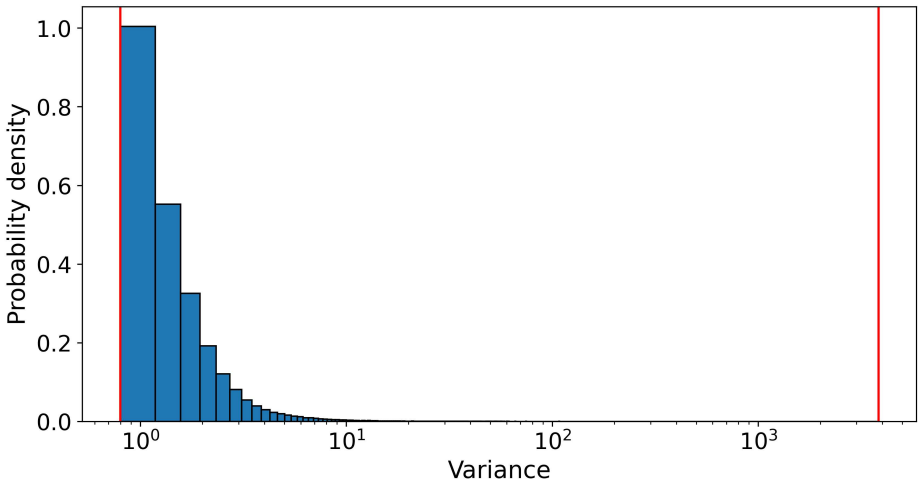

Fig. 3.14 Histogram showing the distribution of the values of $\mathrm{Tr}[F^{-1}]$, sampling uniformly over 100'000 $\underline{\lambda}$ with four probes. In creating this graph, the optimal measure given by Equation 3.4.10 has been used. The two red lines represent the minimum and maximum $\mathrm{Tr}[F^{-1}]$. The 5 max values obtained for $\mathrm{Tr}[F^{-1}]$ are: 361, 367, 727, 1394, 3832.

Doing this we get the new histogram in Figure 3.15. This confirms empirically the fact that every $\underline{\lambda}$ allows small variances with the right states.

Lastly, we conclude our analysis with the case of small λ_j. In particular we consider the case $\lambda_j < 0.3$ for each of the three components. Doing this we get the histogram of Figure 3.16. In particular to produce the histogram we used the four states of Equation 3.1.9, just as the beginning of the analysis. It then appears that, since we get a maximum of $\mathrm{Tr}[F^{-1}] \approx 3$, our four probes are sufficient to estimate $\underline{\lambda}$ in this region. Additionally, we found the remarkable result that 90% of the $\underline{\lambda}$ allows for a precision of $\mathrm{Tr}[F^{-1}] < 1.1$, which is extremely close to the theoretical maximum of $\mathrm{Tr}[Q^{-1}]_{\text{optimal}} = 0.75$.

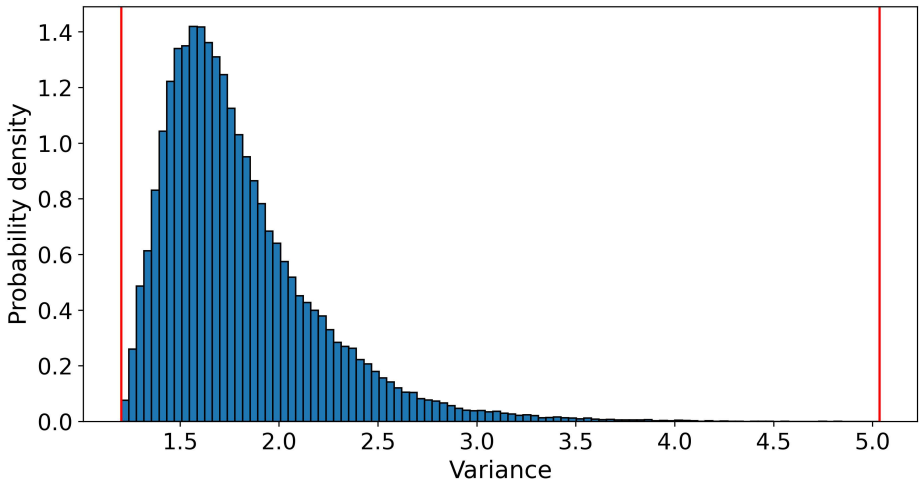

Fig. 3.15 Histogram showing the probability density of a given value of $\mathrm{Tr}[F^{-1}]$, sampling uniformly over 100'000 $\underline{\lambda}$ with 100 probes. In creating this graph, the optimal measure given by Equation 3.4.10 has been used. The two red lines represent the minimum and maximum $\mathrm{Tr}[F^{-1}]$.

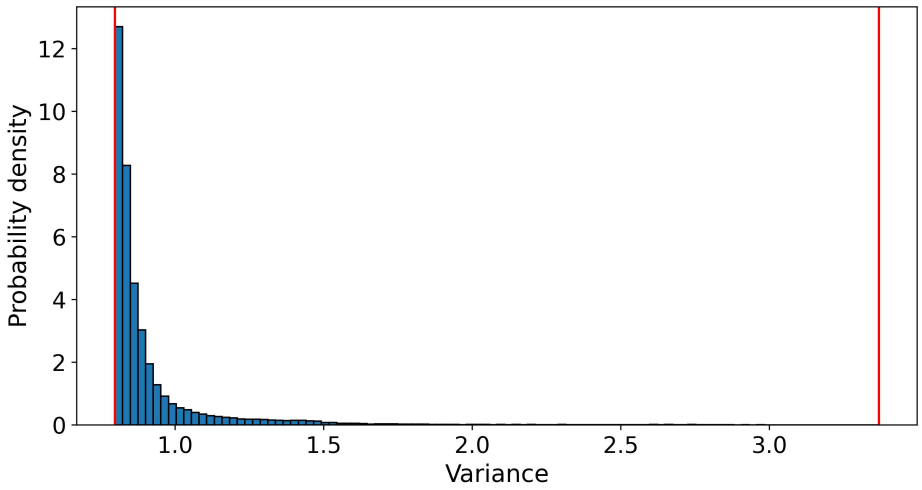

Fig. 3.16 Histogram showing the probability density of a given value of $\mathrm{Tr}[F^{-1}]$, sampling uniformly over 100'000 $\underline{\lambda}$ with four probes, such that $\lambda_j < 0.3$. In creating this graph, the optimal measure given by Equation 3.4.10 has been used. The two red lines represent the minimum and maximum $\mathrm{Tr}[F^{-1}]$. We have that 90% of the $\underline{\lambda}$ allows for $\mathrm{Tr}[F^{-1}] < 1.1$, and 99% of the $\underline{\lambda}$ allows for $\mathrm{Tr}[F^{-1}] < 2$

4

CONCLUSIONS AND PERSPECTIVES

The purpose of the thesis has been to analyze the Cartan's kernel of a generic 2qbit gate. It has been showed that the optimal precision achieved is $\sum_{\lambda_j} \sigma^2_{\lambda_j} = 0.75$, with an information of 64. Additionally it has also been derived the curve with maximum information at fixed trace given by

$$\mathrm{Det}[Q](t) = \frac{\left(-\sqrt{64t^2 - 60t + 9} + 16t - 3\right)\left(\sqrt{64t^2 - 60t + 9} + 8t + 3\right)^3}{36t^4\left(2\sqrt{64t^2 - 60t + 9} + 16t - 3\right)}, \tag{4.0.1}$$

with $t \in [0.75, +\infty)$

Then, we found probe states that allow for such optimality, and suboptimality. Of the former it has also been done an analysis on how generic noise can impact on the precision achievable. It has been found that small noise don't affect too much the precision, under suitable choices of probe parameters. Additionally it has been found a characterization of optimal states, tied to an interpretation of their components as two qbits, as explained in Section 3.1.5.

Lastly, it has been provided a measurement protocol that makes use of local spin measures on the two qbits. The reason for this being the fact that we want simple implementable measures. Despite using suboptimal measures, it allows with good probability a precision roughly similar to the optimal. Ideally it would be interesting finding minimal sets of probes that ensure $\mathrm{Tr}[F^{-1}]$ to be under given thresholds.

Additionally, in the Appendix B it has been briefly addressed the same analysis for qtrits. It has been found that they provide worse performances. It would be interesting formalizing the reason, and possibly generalizing the result for n-dimensional pair of bits.

A

ENTANGLING POWER

In this appendix we will briefly talk about the entangling power of U at different $\underline{\lambda}$. Let's consider a bipartite system with $\mathcal{H} \equiv \mathcal{H}_1 \otimes \mathcal{H}_2 \simeq \mathbb{C}^2 \otimes \mathbb{C}^2$. The definition of entangling power, as provided in [4] is

$$e_p(U) \equiv \overline{E(U|\psi_1 \otimes |\psi_2\rangle\rangle)}^{\psi_1,\psi_2}, \tag{A.0.1}$$

defined to be the average of a given entanglement measure E, over all possible factorizable states $|\psi_1\rangle \otimes |\psi_2\rangle$, distributed with a certain probability density $p(\psi_1, \psi_2)$. We will consider p to be uniform, and the entanglement measure to be the linear entropy defined as

$$E(|\Psi\rangle) \equiv 1 - \mathrm{Tr}_1\Big[\mathrm{Tr}_2^2[|\Psi\rangle\langle\Psi|]\Big]. \tag{A.0.2}$$

We can see that given a bipartite pure quantum system, $0 \leq E \leq 1 - \frac{1}{d}$.

We now consider a space $\mathcal{H}^{\otimes 2}$, onto which we denote T_{jk} the transpositions between the i-th and the j-th factor of $\mathcal{H}^{\otimes 2} \simeq (\mathbb{C}^2 \otimes \mathbb{C}^2) \otimes (\mathbb{C}^2 \otimes \mathbb{C}^2)$. Using this, we define the projectors $P^{\pm}_{jk} \equiv \frac{1}{2}(\mathbb{1} \pm T_{jk})$, over the totally symmetric(antisymmetric) subspaces of $\mathcal{H} \otimes \mathcal{H}$. The space $\mathrm{End}(\mathcal{H}^{\otimes 2})$ is endowed with the Hilbert-Schmidt scalar product $\langle A, B\rangle \equiv \mathrm{Tr}[A^\dagger B]$. Lastly, we define $\mathcal{S}(\mathcal{H})$ as the space of density matrices over $\mathcal{H}$. Using this it is possible to rewrite Equation A.0.1 as

$$e_p(U) \equiv 2\mathrm{Tr}[U^{\otimes 2}\Omega_p U^{\dagger\otimes 2} P^-_{13}], \tag{A.0.3}$$

with

$$\Omega_p \equiv \int d\mu(\psi_1, \psi_2)(|\psi_1\rangle\langle\psi_1| \otimes |\psi_2\rangle\langle\psi_2|)^{\otimes 2} \in \mathcal{S}(\mathcal{H}^{\otimes 2}), \tag{A.0.4}$$

where $d\mu(\psi_1, \psi_2)$ denotes the measure over the product state manifold induced by the probability distribution $p(\psi_1, \psi_2)$.

A.1 ENTANGLING POWER OF U

From the former definitions there are two possible paths. One solely numerical, given by Equation A.0.1. The second is only partially numerical. In fact we see that in Equation A.0.4 we need to calculate Ω_p. After calculating this matrix through numerical methods, we can proceed analytically. The benefit of this second approach is that we get a closed formula, in contrast to the first way where we need to average over all possible states for every $\underline{\lambda}$.
Doing this we end up with the formula

$$e_p(U) = C_0 - C_1 \cos(4\lambda_1)\cos(4\lambda_2) - C_2\Big[\cos(4\lambda_1) + \cos(4\lambda_2)\Big]\cos(4\lambda_3), \qquad \text{(A.1.1)}$$

with $C_0 \equiv 0.1718770625$, $C_1 \equiv 0.1093680225$, $C_2 \equiv 0.03125452$ in simple precision. If we plot this we get Figure A.1

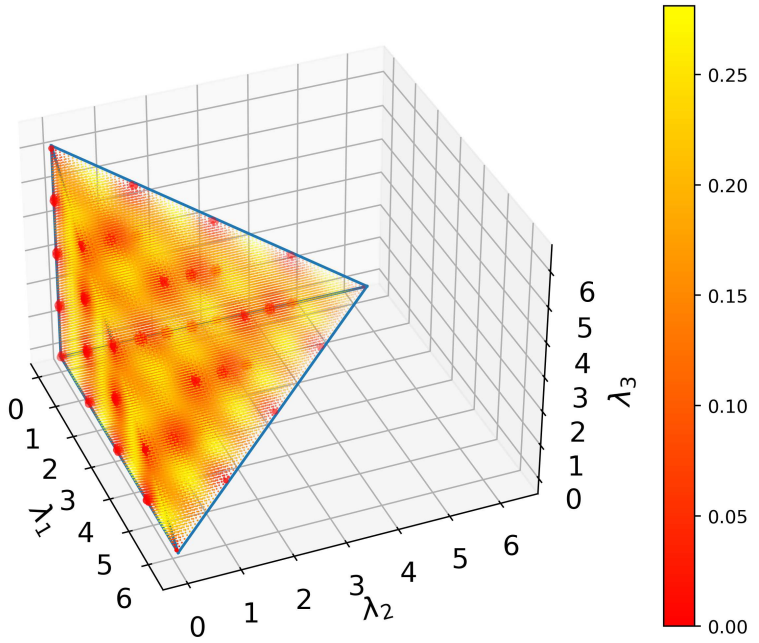

Fig. A.1 Entangling power at different $\underline{\lambda}$, using Equation A.1.1. The shown domain is a cube $[0, 2\pi]^3$ cut in half, in order to show trends inside the cube. As it can be seen the function has a periodicity, therefore the cut part would be symmetrical to the one showed.

B

AN ANALYSIS ON QTRITS

We may ask ourselves if working with systems with more levels could provide better precision. Obviously the least number of levels is 2. This case has been analyzed in the thesis. We now analyze the case $d = 3$.

B.1 CARTAN'S KERNEL FOR QTRITS

First of all we need to know the new kernel. To calculate it we now take the matrices relative to spin 1

$$S_1 \equiv \begin{pmatrix} 0 & 1 & 0 \\ 1 & 0 & 1 \\ 0 & 1 & 0 \end{pmatrix}/\sqrt{2}, \quad S_2 \equiv \begin{pmatrix} 0 & -i & 0 \\ i & 0 & -i \\ 0 & i & 0 \end{pmatrix}/\sqrt{2}, \quad S_3 \equiv \begin{pmatrix} 1 & 0 & 0 \\ 0 & 0 & 0 \\ 0 & 0 & -1 \end{pmatrix}. \tag{B.1.1}$$

Using these, the new kernel is given by

$$U \equiv e^{-i \sum_{j=1}^{3} \lambda_j S_j}. \tag{B.1.2}$$

To avoid excessive complexity we work in the diagonal base. Diagonalizing the exponent, and exponentiating it we get

$$U = \begin{pmatrix} e^{-i\lambda_1} & 0 & 0 & 0 & 0 & 0 & 0 & 0 & 0 \\ 0 & e^{i\lambda_1} & 0 & 0 & 0 & 0 & 0 & 0 & 0 \\ 0 & 0 & e^{-i\lambda_2} & 0 & 0 & 0 & 0 & 0 & 0 \\ 0 & 0 & 0 & e^{i\lambda_2} & 0 & 0 & 0 & 0 & 0 \\ 0 & 0 & 0 & 0 & e^{-i\lambda_3} & 0 & 0 & 0 & 0 \\ 0 & 0 & 0 & 0 & 0 & e^{i\lambda_3} & 0 & 0 & 0 \\ 0 & 0 & 0 & 0 & 0 & 0 & e^{-iA} & 0 & 0 \\ 0 & 0 & 0 & 0 & 0 & 0 & 0 & e^{-iB} & 0 \\ 0 & 0 & 0 & 0 & 0 & 0 & 0 & 0 & e^{iC} \end{pmatrix}, \tag{B.1.3}$$

with

$$\begin{aligned} A &= \frac{2\sqrt{\lambda_1^2+\lambda_2^2+\lambda_3^2}\sin\left(\frac{1}{3}\mathrm{Arg}\left[f+9i\Lambda\right]\right)}{\sqrt{3}} \\ B &= \frac{6\Lambda+\left(\lambda_1^2+\lambda_2^2+\lambda_3^2\right)^{3/2}\left(\sqrt{3}\sin\left(\frac{1}{3}\mathrm{Arg}\left[f+9i\Lambda\right]\right)+3\cos\left(\frac{1}{3}\mathrm{Arg}\left[f+9i\Lambda\right]\right)\right)}{\left(\lambda_1^2+\lambda_2^2+\lambda_3^2\right)\left[\sqrt{3}\sin\left(\frac{2}{3}\mathrm{Arg}\left[f-9i\Lambda\right]\right)-\cos\left(\frac{2}{3}\mathrm{Arg}\left[f-9i\Lambda\right]\right)-2\right]} \\ C &= \frac{6\Lambda+\left(\lambda_1^2+\lambda_2^2+\lambda_3^2\right)^{3/2}\left(\sqrt{3}\sin\left(\frac{1}{3}\mathrm{Arg}\left[f+9i\Lambda\right]\right)-3\cos\left(\frac{1}{3}\mathrm{Arg}\left[f+9i\Lambda\right]\right)\right)}{\left(\lambda_1^2+\lambda_2^2+\lambda_3^2\right)\left[\sqrt{3}\sin\left(\frac{2}{3}\mathrm{Arg}\left[f-9i\Lambda\right]\right)+\cos\left(\frac{2}{3}\mathrm{Arg}\left[f-9i\Lambda\right]\right)+2\right]} \end{aligned} \tag{B.1.4}$$

with

$$\begin{aligned} f \equiv f(\underline{\lambda}) &= \sqrt{3}\sqrt{\left(\lambda_1^2+\lambda_2^2+\lambda_3^2\right)^3-27\lambda_1^2\lambda_2^2\lambda_3^2} \\ \Lambda \equiv \Lambda(\underline{\lambda}) &= \lambda_1\lambda_2\lambda_3 \end{aligned} \tag{B.1.5}$$

B.2 QTRIT ANALYSIS

From here the possible approaches are two. The first is observing that the upper block of the first 6 components is algebraically simple. It can be also seen that its eigenvectors are simple too. Therefore, one could analyze the problem analytically

working only in this subspace.
On the other hand, by sacrificing analytical results, it is possible to conduce the analysis on the whole space numerically.

B.2.1 *Analytical approach*

We define the initial state to be

$$|\psi\rangle = \begin{pmatrix} a \\ be^{i\phi_b} \\ ce^{i\phi_c} \\ de^{i\phi_d} \\ ee^{i\phi_e} \\ fe^{i\phi_f} \end{pmatrix}, \tag{B.2.1}$$

expressed in the diagonal base. If we now evolve the state using the upper block of Equation B.1.3, and calculate the QFI via 2.1.7, we get

$$Q = \begin{pmatrix} Q_{11} & Q_{12} & Q_{13} \\ Q_{21} & Q_{22} & Q_{23} \\ Q_{31} & Q_{32} & Q_{33} \end{pmatrix}, \tag{B.2.2}$$

with

$$\begin{aligned} Q_{11} &= 4\left(-a^4 + a^2\left(2b^2+1\right) - b^4 + b^2\right) \\ Q_{22} &= 4\left(-c^4 + c^2\left(2d^2+1\right) - d^4 + d^2\right) \\ Q_{33} &= 4\left(-e^4 + e^2\left(2f^2+1\right) - f^4 + f^2\right) \\ Q_{12} &= Q_{21} = -4(a-b)(a+b)(c-d)(c+d) \\ Q_{13} &= Q_{31} = -4(a-b)(a+b)(e-f)(e+f) \\ Q_{23} &= Q_{32} = -4(c-d)(c+d)(e-f)(e+f). \end{aligned} \tag{B.2.3}$$

The trace of its inverse is

$$\mathrm{Tr}[Q^{-1}] = -\frac{4a^2b^2\left(a^2+b^2-1\right)+3AB\left(c^2+d^2\right)+4Ae^2f^2+3B\left(c^4+d^4\right)+2c^2d^2C}{16\left(a^2b^2Bc^2+a^2b^2Bd^2+f^2\left(a^2+b^2\right)\left(c^2\left(d^2+e^2\right)+d^2e^2\right)+a^2c^2d^2e^2+b^2c^2d^2e^2\right)}, \tag{B.2.4}$$

with

$$\begin{aligned} A &\equiv -1+e^2+f^2 \\ B &\equiv e^2+f^2 \\ C &= 2c^2+2d^2+3e^2+3f^2-2 \end{aligned} \tag{B.2.5}$$

and its determinant is

$$\begin{aligned} \mathrm{Det}[Q] = &-64\left(a^2+b^2\right)\left(c^2-d^2\right)^2\left(e^2-f^2\right)^2-64\left(a^2-b^2\right)^2\left(c^2+d^2\right)\left(e^2-f^2\right)^2+ \\ &4\left(-e^4+e^2\left(2f^2+1\right)-f^4+f^2\right)\left[16\left(-a^4+a^2\left(2b^2+1\right)-b^4+b^2\right)\right. \\ &\left.\left(-c^4+c^2\left(2d^2+1\right)-d^4+d^2\right)-16\left(a^2-b^2\right)^2\left(c^2-d^2\right)^2\right]. \end{aligned} \tag{B.2.6}$$

We can see the neither of the two depends on $\underline{\lambda}$, just as the qbit case.

B.2.2 *Numerical approach*

Here we can proceed just as the subsection before, with the advantage that now we do not need to keep track of equations. In fact through the expression of U, we can calculate $|\psi_{\underline{\lambda}}\rangle \equiv U|\psi\rangle$. With this, by calculating derivatives numerically we can get the QFI, and from that the trace of its inverse and the determinant.

By putting together the numerical approach and the analytical one, we get Figure B.1, where we plot points in the trace determinant plane, comparing the performances of the two approaches.

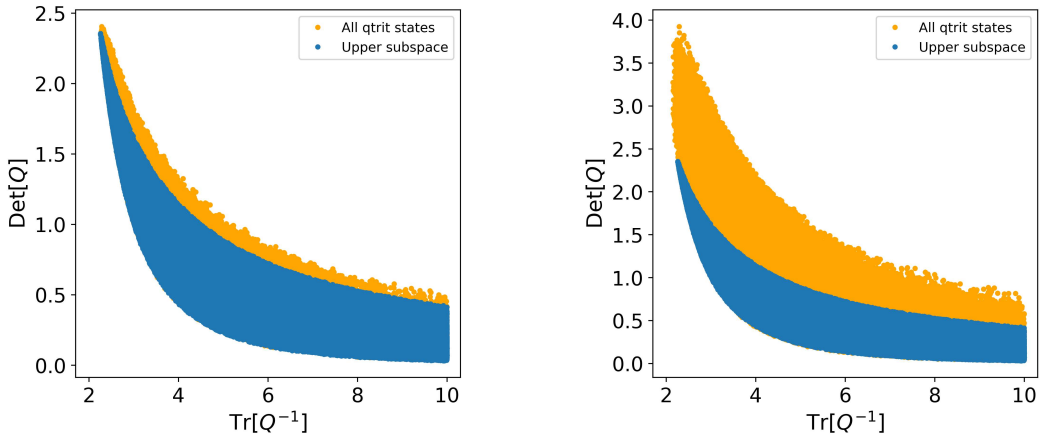

Fig. B.1 Trace and determinant achievable through different qtrit probe states. The orange are points reached by considering all possible probes, while the blue are a subclass of points, reached only by states with null components in the last 3 components of the vector expressed in the base that diagonalize U. For this reason, beneath every blue region there is also an orange one. To be noted how the total $\mathrm{Tr}[Q^{-1}]$ is dependent on $\underline{\lambda}$. Despite this, we get similar images at various $\underline{\lambda}$. The left panel is calculated with $\underline{\lambda} = (1.9, 5.6, 4.1)$, while the right one with $\underline{\lambda} = (10^{-7}, 10^{-7}, 10^{-7})$, both realized with around 150'000 orange points, and 600'000 blue ones. Just as in the qbit case, the image has been limited by $\mathrm{Tr}[Q^{-1}] < 10$ due to aesthetical reasons.

From Figure B.1 we can observe two things. The first is that the subspace performs worse. The second is that both achieve optimality at around Tr = 2.1. This is higher with respect to the 0.75 achieved by qbits. Also, the information is less, being around $2 \sim 4$ at best, with respect to the 64 of qbits. Additionally, one thing that must be mentioned is that contrary to the subspace, the total Q depends on $\underline{\lambda}$. This makes so that at different $\underline{\lambda}$ we get different orange sets. In particular, we see that the orange set spans from being equal to the blue set, roughly up to what is showed in the right panel of Figure B.1, with $\underline{\lambda} = (10^{-7}, 10^{-7}, 10^{-7})$. Despite these differences, all possible $\underline{\lambda}$ have an optimal precision that is worse than the qbit case. In conclusion, we have that qtrits doesn't provide better precision.

REFERENCES

[1] Robert R. Tucci. An introduction to cartan's kak decomposition for qc programmers. *arXiv: Quantum Physics*, 2005.

[2] Jing Liu, Haidong Yuan, Xiao-Ming Lu, and Xiaoguang Wang. Quantum fisher information matrix and multiparameter estimation. *Journal of Physics A: Mathematical and Theoretical*, 53(2):023001, December 2019.

[3] Sholeh Razavian, Matteo G. A. Paris, and Marco G. Genoni. On the quantumness of multiparameter estimation problems for qubit systems. *Entropy*, 22(11):1197, October 2020.

[4] Paolo Zanardi, Christof Zalka, and Lara Faoro. Entangling power of quantum evolutions. *Physical Review A*, 62(3), August 2000.

ACKNOWLEDGEMENTS

I would like to express my gratitude for all the people around me, who supported me and made my journey possible. First of all a special thanks to professor Matteo G. A. Paris, for his expert guidance, and dedicated mentorship, who helped me navigate in a new interesting field of study.

Additionally, I am grateful for my whole family's support, without which this would not have been possible. A special thanks to my brother Matteo, and my parents Franco and Laura.

Finally, a special thanks to all the people who surrounded me every day, and in particular the companions and friends with whom I've shared this journey: Alice, Edoardo, Gabriele, Ivan, Leo, Ludovico, Michele and Pietro.